# Perilipin membrane-association determines lipid droplet heterogeneity in differentiating adipocytes

Mario Majchrzak[2], Ozren Stojanovic[1], Dalila Ajjaji[3], Kalthoum Ben M'barek[3], Mohyeddine Omrane[3], Abdou Rachid Thiam[3], Robin W. Klemm[1,2,4,5]

[1]Department of Physiology Anatomy and Genetics, University of Oxford, Oxford OX1 3PT, UK
[2]Department of Molecular Life Sciences, University of Zurich, 8057 Zurich, CH
[3] Laboratoire de Physique de l'École Normale Supérieure, ENS, Université PSL, CNRS, Sorbonne Université, Université de Paris, F-75005 Paris, France
[4]Correspondence : Robin.Klemm@dpag.ox.ac.uk
[5]Lead contact

**Summary**

The storage of fat within lipid droplets (LDs) of adipocytes is critical for whole-body health. Acute fatty acid uptake by adipocytes leads to the formation of at least two LD-classes marked by distinct members of the perilipin (PLIN) protein-family. How LD-heterogeneity arises is an important yet unresolved cell biological problem. Here, we show that an unconventional integral membrane-segment targets the adipocyte specific LD-surface factor PLIN1 to the endoplasmic reticulum (ER) and binds with high affinity to the first LD-class. The other PLINs do not insert into the ER and remain cytoplasmic until fatty acid influx recruits them to a newly forming LD-population. Preventing ER-localization turns PLIN1 into a cytoplasmic LD-protein, reduces its LD-affinity and switches its LD-class specificity. Our results explain how differences in organelle targeting and disparities in lipid-affinity of LD-surface factors establish LD-heterogeneity. These findings have direct implications for mechanism-based interference with fatty-liver disease, type-2 diabetes and obesity.

## Introduction

Adipocytes deposit an excess of dietary nutrients as triacylglycerols (TAGs) in large lipid droplets (LDs) and release fatty acids to feed other tissues during fasting[1–3]. Deficiencies in LD biogenesis and turnover, or defects in factors important for LD surface assembly are associated with several metabolic diseases such as lipodystrophies, fatty liver disease, type-2 diabetes, and obesity[4–6].

LDs form at the membranes of the endoplasmic reticulum (ER) when neutral lipids, such as TAGs, accumulate between the two leaflets of the lipid bilayer[7–9]. With increasing TAG amounts, they phase-separate from the phospholipids in the membrane to form lenses or TAG-inclusions, which eventually bud out into the cytoplasm giving rise to LDs. As a result, the LD-surface is surrounded by a phospholipid monolayer and a set of LD specific surface proteins[10–14].

Early models in the field suggested that all LDs within a cell have the same lipid and protein composition and carry out similar functions. Accumulating evidence suggests, however, that LDs are highly heterogenous, and can specialize into different sub-populations which are morphologically, chemically, and functionally distinct[14–21].

One way by which cells can generate different LD-classes is determined by the pathways that synthesize the lipids in the hydrophobic core of the LD. For example, fly fat bodies contain a population of large LDs in the center of the cell, which is mostly filled with TAGs derived from *de novo* lipogenesis, i.e. the synthesis of fatty acids from non-lipid precursors such as glucose[22,23]. A class of smaller LDs in the periphery of the cell seems more specialized in storing TAGs made from fatty acids that are taken up from the outside[22,23]. Consistent with the work in flies, fatty acid feeding of mammalian adipocytes has long been known to lead to the formation of two distinct LD-classes[10,24,25]. As in flies the central LD population is formed mainly by *de novo* lipogenesis [26], whereas acute fatty acid influx appears to trigger the formation of a second LD class in the periphery of the cell[10,24,25]. However, the mechanisms that lead to the formation of different LD populations remain poorly understood, and current models of LD-biogenesis do not explain how LD-surface factors can be targeted to a specific LD population in the cell.

In general, protein targeting to LDs occurs by two major pathways[14,27,28]. Class I (or ERTOLD) proteins are synthesized as monotopic integral membrane proteins at the ER, and subsequently move to the LD surface (**Fig. 1A**, class I). The dual localization to the ER and the LDs is facilitated by special membrane anchors that often appear to fold into hairpin-like conformations and are characterized by signature residues such as internal prolines and tryptophans as well as positively charged residues[13,28].
Class II (or CYTOLD) proteins, on the other hand, bind directly from the cytoplasm to the LD surface (**Fig. 1A,** class II). They do not possess integral membrane segments and are instead targeted to the LD by amphipathic domains that detect packing defects in the LD monolayer where the hydrophobic LD core is exposed to the cytoplasm[14,29–34].

The perilipins (PLINs) are currently viewed as the prototypical class II proteins, comprising a family of evolutionarily conserved LD-surface factors carrying out important structural and regulatory functions[25,35–38]. The family defining N-terminal PAT domain and the following 11-mers both contain amphipathic regions, which are critical for LD-targeting (**Fig. S1A**)[31,36,39,40]. All five perilipin family members are thought to target the LD directly from the cytoplasm and should

therefore freely mix on the same LD class. In contrast to this expectation, the LD sub-populations that form in adipocytes upon fatty acid feeding are marked by specific PLINs (**Fig. 1B**) [10,24,25]. An affinity-based LD binding "hierarchy" among the different PLIN-family members is likely key to the formation of the two LD classes[33,39,41–44]. However, the molecular mechanisms leading to class-specific localization of LD surface proteins are not well understood, and the biochemical characterization of the responsible targeting domains remains incomplete[37].

## Results

### Acute fatty acid feeding induces the formation of distinct LDs in adipocytes

To investigate how perilipins (PLINs) target LDs in adipocytes, we differentiated 3T3-L1 cells into white adipocytes and visualized endogenously expressed PLIN1, 2, 3, and 4 after fatty acid feeding by immunofluorescence (PLIN5 is not expressed in 3T3-L1 adipocytes [11,26]). Our data showed that adipocytes form two separate LD populations under these conditions (**Fig. 1B-F**) confirming previous observations[25,35,38,39,41]. The LDs in the centre of the cell were almost exclusively labelled with PLIN1, and the second population localizing more to the periphery was preferentially bound by PLIN2, 3, and 4 (Fig. 1C, D, and E). While the central population was specifically marked by PLIN1 (Fig. 1 C-F), the peripheral LD population was more heterogenous, and was either exclusively marked by PLIN2, 3, and 4, or additionally contained some PLIN1, which we therefore classified as a mixed LD population (**Fig. 1C-E** (zoom-ins), **F** (MIX)).

Consistent with our results in adipocytes and the established LD binding hierarchy in other cells[25,42], we next showed that ectopically expressed PLIN1 excluded PLIN2, 3, or 4 from LDs when co-transfected in COS7 cells (**Fig. S1A-D**). As predicted, the high LD-affinity of PLIN1 was dependent on features C-terminally of the 11-mer domain (**Fig. S1A**). A construct only consisting of the N terminal PAT and 11-mer regions (PLIN1 1-192) was not able to exclude PLIN2 from the LD surface (**Fig. S1E**). In fact, in most of the cells expressing both constructs, PLIN2 excluded the PLIN1 truncation mutant (PLIN1 1-192) from the LD surface indicating higher affinity (**Fig. S1E**). Together these data raised the question of how class-II LD proteins can separate onto two different LD-populations within the same cell, and which domains in PLIN1 are required for this behaviour.

### PLIN1 is an integral membrane protein dually localizing to the ER and LDs

To determine the molecular basis of LD targeting by the PLINs, we examined PLIN1 and 2 by biochemistry and microscopy experiments expressing them alone in otherwise untreated COS7 cells. As expected, PLIN1 localized to endogenous LDs but was, surprisingly, never seen in the cytoplasm. Instead, it always bound to the ER (**Fig. 2A, Fig. S2B**). In agreement with data from others[44], our results indicated that PLIN1 does not behave as a prototypical class-II LD protein. PLIN2, however, showed normal class-II behaviour accumulating in the cytoplasm upon overexpression and covering all endogenous LDs (**Fig. 2B, S2A, S2D**). After addition of fatty acid ($Na^+$ oleate), both PLIN1 and PLIN2 targeted efficiently to LDs (**Fig. 2C, and D**). Only around 10 % of the cells showed some residual ER-staining for PLIN1 (**Fig. 2E**).

128 Since PLIN1 does not contain any predicted membrane segments (**Fig. S2D, S2E**), and
129 exhibits similar overall hydrophobicity as PLIN2 (**Fig. S2F, S2G**), we initially expected that it would
130 bind the ER as a peripheral membrane protein or would associate with membranes through a
131 receptor in the ER. In support of this view, PLIN1 sedimented both as an untagged and GFP-fusion
132 protein together with the endogenously expressed integral ER membrane protein calnexin (CNX)
133 to the membrane pellet (**Fig. 2F**, PLIN1 untagged; GFP-PLIN1, P100, consistent with ER in[44]).
134 However, when we subjected the membrane pellet (P100) to alkaline extraction with $Na_2CO_3$-
135 buffer, PLIN1 quantitatively remained in the alkaline resistant membrane fraction (**Fig. 2F**, P100E)
136 behaving like an integral membrane protein. PLIN2, on the other hand was absent from the
137 membrane fractions and as expected for a canonical class-II protein, it co-fractionated with the
138 soluble cytoplasmic marker glyceraldehyde-3-phosphate dehydrogenase (GAPDH, **Fig. 2F**, S100).
139 To exclude possible artefacts, we additionally carried out flotation experiments. To this
140 end, we prepared a ribosome stripped membrane fraction from cells expressing PLIN1 and
141 loaded it to the bottom of a sucrose step gradient. As shown in **Fig. 2G**, PLIN1 moved efficiently
142 out of the bottom fraction and floated together with ER membranes to an interface fraction
143 marked by CNX (5-35% sucrose). When we solubilized the membrane pellet with detergent,
144 neither PLIN1 nor CNX floated (**Fig. 2H**). Finally, PLIN1 and CNX both remained soluble when we
145 mixed the cell lysate with detergent before high-speed centrifugation (**Fig. 2I**).
146 Taken together, the imaging and biochemical data indicated that PLIN1 is an integral ER
147 membrane protein and does not belong to the cytoplasmic class-II proteins. The targeting
148 pathway to the LD might therefore be more complex than currently envisaged, probably involving
149 the ER as an intermediate step. In support of this notion, we found that PLIN1 moved efficiently
150 onto LDs when we blocked translation with cycloheximide 1h before LD induction (**Fig. S2H-J**).
151 The ER-pool re-distributed efficiently to the LDs (**Fig. 2J**).
152
153 **PLIN1 contains an unconventional integral membrane segment and a peripheral membrane**
154 **binding motif**

155 To explore the molecular basis of the subcellular localization of PLIN1 in more detail, we
156 next aimed at identifying the domains that are required for membrane targeting. We, therefore,
157 carried out a systematic structure-function analysis using fluorescence microscopy and
158 subcellular fractionation followed by alkaline extraction to probe for membrane integration.
159 We started the analysis with a minimal N-terminus of the mouse PLIN1 sequence (PLIN1
160 1-192) containing the PAT and 11-mer regions that were previously shown to be sufficient for LD
161 targeting (**Fig. S3A**)[31,39,42]. As expected, neither of these two domains nor a polybasic region
162 enriched in prolines downstream of the 11-mer region was involved in ER targeting. In fact, the
163 N-terminal PLIN1 portion until position 237 remained completely soluble (**Fig. 3A**, S100) and was
164 found in the cytoplasm as well as on the endogenous LDs (**Fig. 3B, S3B**).
165 However, a construct extended until residue 281 (PLIN1 1-281) pelleted efficiently to the
166 membrane fraction P100, and was alkaline resistant (**Fig. 3A**, P100E). This construct also localized
167 to the ER as determined by microscopy, indicating that the region between residues 238 and 280
168 contained an integral membrane segment (iMS) (**Fig. 3A** green domain, and **S3B**). Interestingly,
169 the corresponding C-terminal portion (PLIN1 281-517) was found in the supernatant S100 (**Fig.**
170 **3A**) but localized to the ER as shown by microscopy (**Fig. 3D**), suggesting that PLIN1 contains an

171 additional peripheral membrane segment (pMS) that contributes to ER binding. Computational
172 analysis of the C-terminal portion predicted a strong amphipathic region in a segment between
173 residues 380 and 400 (**Fig. 3A**, yellow). However, a construct containing this motif (Plin1 371-517)
174 remained completely soluble in the cytoplasm (**Fig. 3A, and 3E**). Further extension of the C-
175 terminal part just until the beginning of the 4-helix bundle (PLIN1 328-517) led to ER localization
176 (**Fig. 3F**), but this construct remained soluble in the fractionation experiments (**Fig. 3A**), indicating
177 that the potential pMS is positioned in this first section of the middle domain (**Fig. 3A**, orange).
178 To narrow down the two membrane binding regions further, we turned to hydropathy
179 plot analysis (**Fig. S2F**). A first segment with moderate hydrophobicity was found between
180 tryptophan 238 and proline 280 of the mouse PLIN1 sequence, corresponding to the region in
181 which we identified the iMS (**Fig. S2F and 3G**). Although slightly less hydrophobic than the first
182 segment, a second region between residues 348 and 370 coincided with the peripheral
183 membrane segment (pMS, **Fig. S2F and 3G**).
184 To test the function of these domains in ER targeting we deleted them from the PLIN1
185 sequence. PLIN1ΔΔ lacking both the iMS and the pMS (**Fig. 3G**, PLIN1 Δ238-280, Δ348-370) was
186 completely soluble, and showed no membrane association after high-speed membrane
187 sedimentation or in the flotation experiments (**Fig. 3H**). Additionally, this mutant localized to the
188 cytoplasm in all cells that expressed the construct (**Fig. 3I**). Although having lost its ability to bind
189 the ER, PLIN1ΔΔ was still found on LDs after fatty acid feeding, but did not exclude PLIN2
190 anymore, which was now often found on the same LDs (**Fig. 3J**). In conclusion, removal of the
191 iMS and the pMS converted PLIN1 into a class II LD-protein, targeting LDs directly from the
192 cytoplasm (**Fig. 3K**).
193
194 In agreement with these results, addition of the iMS to PLIN2, right downstream of the
195 11-mer region (PLIN2-iMS (insertion at position 251)), was sufficient for membrane integration
196 (**Fig S3C, S3D, S3E**). ER-insertion of PLIN2-iMS simultaneously increased LD affinity, and permitted
197 efficient competition with PLIN1 for LD formation at the ER (**Fig. S3E**). However, PLIN2-iMS did
198 not mix with PLIN1 on the same LDs, but tended to segregate onto a separate LD class (**Fig. S3E**),
199 indicating a critical function for the iMS in the nucleation of different LD populations at the ER.
200
201 Taken together our data show that PLIN1 behaves as an integral ER membrane protein
202 that can move to LDs showing characteristic of a class-I rather than a class-II LD-protein. Both the
203 iMS and the pMS are sufficient for ER targeting, but membrane integration, and the generation
204 of different LD-classes depend on the iMS. Removing the ability to integrate into the ER converts
205 PLIN1 into a conventional class II LD-protein. The ER-binding deficient PLIN1-mutant mixes better
206 with class II-PLINs on the same LDs indicating that it has reduced LD affinity.
207
208
209
210
211
212
213
214

215 **The iMS is critical in determining PLIN1 LD-binding kinetics**

216 To investigate this possibility biochemically, we analysed the monolayer affinity of PLIN1
217 and PLIN1ΔΔ *in vitro*, using an assay that mimics the LD surface (**Fig. 4A**,[30]). Shrinkage of the
218 aqueous compartments in this buffer-in-oil system leads to compression of the artificial LD-
219 monolayer at the oil-buffer interface. The proteins fall off the monolayer with progressive
220 reduction of the interface area and accumulate proportionally to their off-rates in the buffer
221 compartment[30]. In agreement with the microscopy and fractionation experiments (**Fig. 3G-K**, and
222 [39,41]), full-length PLIN1 remained efficiently bound to the interface of the buffer compartment,
223 indicating that the high LD affinity is determined by low off-rates from the monolayer (**Fig. 4, B**).
224 In comparison, PLIN1ΔΔ readily fell off the interface when the aqueous phase began to shrink,
225 showing faster off-rates and lower affinity to the monolayer than full-length PLIN1 (**Fig. 4A, B**).
226 The progressive accumulation in the buffer phase with increasing monolayer compression further
227 showed that PLIN1 excluded PLIN1ΔΔ from the LD surface mimic, confirming the results in cells
228 (**Fig. 4A, B**).
229 To gain insights into the corresponding on-reaction of the binding equilibrium, we used
230 fluorescence recovery after photobleaching experiments in cells. Deletion of either the iMS
231 (PLIN1ΔiMS) alone or together with the pMS (PLIN1ΔΔ) made recovery on the LD faster by more
232 than an order of magnitude compared to a mutant in which the iMS is present and only the pMS
233 is removed (PLIN1ΔpMS) (**Fig. 4C**, still frames of time series **Fig. S4A**). Together these results
234 suggest that PLIN1 binds LDs with both low off and on rates, which is determined by the iMS. LD-
235 binding and exchange via the classical amphipathic segments on the other hand appears to be
236 faster, but results, overall, in lower LD-affinity.
237 These data suggested that differences in membrane targeting and LD-affinity by the PLINs
238 may provide a simple explanation for the formation of the two LD populations in adipocytes:
239 PLIN1 is targeted to the ER via the iMS where it binds to the emerging LDs first, excluding the
240 low-affinity PLINs from the surface of this LD class. However, due to its high affinity, PLIN1 is
241 "trapped" on this first LD population and is therefore not able to re-distribute fast enough to the
242 second LD-class which acutely appears upon fatty acid feeding. Since PLIN2, 3 and 4 are excluded
243 from the LDs that are covered by PLIN1, they remain available in the cytoplasm and can readily
244 bind to the surface of these newly synthesized LDs. Despite their lower LD-affinity, the class-II
245 PLINs would label the acutely emerging LD-population first.
246
247 **Perturbation of PLIN1 membrane targeting leads to a LD-class switch in adipocytes**

248 To test these interpretations of the *in vitro* experiments directly in adipocytes, we stably
249 integrated GFP-PLIN1 and GFP-PLIN1ΔΔ as inducible transgenes into our preadipocytes (3T3-L1
250 cells). Consistent with the results above, PLIN1ΔΔ remained soluble in fractionation and alkaline
251 extraction experiments (**Fig. 4D**), and full-length PLIN1 indeed behaved like an integral
252 membrane protein sedimenting to the alkaline resistant membrane pellet, marked here by the
253 endogenously expressed ER membrane protein CLIMP63 (**Fig. 4D and 4E**). PLIN1 localized to LDs
254 after fatty acid feeding and as in COS7 cells moved from the ER to LDs even when translation was
255 shut off with cycloheximide before LD induction (**Fig. S4B-E**).
256 When we induced expression of the transgenes in adipocytes, 6 days post differentiation,
257 PLIN1ΔΔ behaved like a class-II LD protein mostly remaining cytoplasmic and being largely

258 excluded from the big LDs which formed during differentiation (**Fig. 4E and F**). Flotation
259 experiments with extracts from the same adipocytes revealed that endogenous PLIN1 was
260 expressed and floated with the LDs to the top fraction (**Fig. 4G**). PLIN1ΔΔ, was additionally found
261 abundantly in the soluble middle fraction, confirming the microscopy experiments (**Fig. 4E and**
262 **F**). Although being effectively excluded from the LDs covered by endogenous PLIN1, PLIN1ΔΔ
263 remains LD binding competent in cells and *in vitro* (**Fig. 3J, Fig. 4A**). PLIN1ΔΔ probably gained
264 access to the LD core via its amphipathic PAT domain when the LD surface was disrupted during
265 preparation of the cell extracts by mechanical lysis and was therefore also seen in the LD fraction
266 on top of the gradient (**Fig. 4G**).
267 Importantly, PLIN1ΔΔ efficiently moved from the cytoplasm to the peripheral LD
268 population which forms after fatty acid feeding (**Fig. 4H and F**). Consistent with the results shown
269 for PLIN2-4 in **Fig. 1**, PLIN1ΔΔ remained largely excluded from the LDs that were covered by
270 endogenously expressed full-length PLIN1 (**Fig. 4H and F**).
271
272 Taken together, these data suggest that removing the iMS and pMS not only reduced LD
273 affinity and turned PLIN1ΔΔ into a class-II LD-protein, but also leads to a change in LD-class
274 specificity. Moreover, these results are consistent with a model by which the high LD affinity of
275 PLIN1 depends on the membrane targeting segments, particularly the iMS (**Fig. S4F**).
276
277 Finally, we examined the localization of endogenously expressed PLIN1 during adipocyte
278 differentiation. As expected, six days post differentiation, PLIN1 localized almost exclusively to
279 the surface of LDs (**Fig. 4I**). However, at earlier days in the time course, e.g. at day 3 post
280 differentiation, the endogenous PLIN1 pool was additionally abundantly present on the
281 peripheral ER (**Fig. 4J**). Since the ER of adipocytes is structurally less defined than in other
282 cells[10,43,44], and the staining of the membrane is less clear than in other cells, it was critical to
283 additionally probe the membrane association biochemically. Consistent with the imaging results,
284 the PLIN1 membrane pool was completely alkaline-resistant, and pelleted together with the
285 integral ER marker CNX to the bottom of the tube (**Fig. 4L)**. At this stage of the differentiation,
286 PLIN1 is likely produced in excess and is stock-piled in the ER to provide a readily available pool
287 of building blocks for rapid expansion of the LD-surface as the cells synthesize TAGs and the LDs
288 grow at high rate.
289 Interestingly, when we stimulated lipolysis in these cells triggering breakdown of the LDs,
290 PLIN1 efficiently moved back to the ER (**Fig. 4K**) and remained integral to the membrane as shown
291 by alkaline extraction (**Fig. 4K-L**). The interpretation that PLIN1 moves in these cells between the
292 LDs and the ER was further supported by flotation experiments, showing that stimulation of
293 lipolysis re-distributed PLIN1 away from the remaining floating LDs into the membrane pellet at
294 the bottom of the tube (**Fig. 4M**).
295
296
297
298
299
300

## Discussion

Here, we have shown that ER membrane integration and high LD-affinity of PLIN1 are necessary for the formation of LD heterogeneity in adipocytes. In contrast to its previous classification as a cytoplasmic, class-II LD protein (CYTOLD proteins), we have found that PLIN1 in fact behaves like an integral ER membrane protein. We show that an unconventional integral membrane segment (iMS) is necessary and sufficient for integration into the ER membrane and mediates at the same time high LD-affinity.

Our imaging and fractionation experiments with early adipocytes revealed that endogenously expressed PLIN1 is abundantly present in the ER and readily moves to the LD-class that emerges during the differentiation time course. Due to its high affinity, PLIN1 excludes the other PLINs from the surface of this first LD-class, already from the earliest stages in the biosynthesis process. The high LD-affinity is likely necessary to protect the *de novo* synthesized TAGs from turnover by lipases and is therefore required for efficient LD-growth. However, in later stages of adipocyte differentiation, the high LD-affinity has a "trade-off": starting from around day 6, the cellular PLIN1 pool is almost completely found on the surface of the existing LDs and the ER pool is reduced to a minimum. Under these conditions the PLIN1-LDs mostly grow through fusion mediated by CIDE-C and for a so far unknown reason are not able to incorporate new TAGs at high rates. During an acute burst of TAG synthesis, the cell rather forms a second LD population. Since the high LD-affinity "traps" PLIN1 on the surface of the first LD-class it is unavailable for association with the rapidly expanding surface of the second LD-class that form upon fatty acid uptake. This second LD-population is, therefore, primarily covered with the other PLIN-family members thus forming a separate LD class – the class-II LDs. Although class-II PLINs have lower affinity for LDs, they bind faster to the newly emerging LDs because they move onto the expanding LDs directly from the cytoplasm and do not have to take a de-tour through the ER.

Whether PLIN1 LD-targeting follows the same pathway as conventional class-I proteins (ERTOLD proteins) remains to be clarified (**Fig. S4F, ER→LD)**. The length of the hydrophobic region within the iMS of around 30 amino acids (**Fig. S4G**) corresponds to sizes of known hairpin motifs, but the iMS exhibits surprisingly low hydrophobicity and does, therefore, not satisfy the basic definition of a conventional ER membrane anchor[45–47]. The low hydrophobicity is probably also the reason why the iMS is computationally not predicted as an integral membrane segment. However, the iMS contains some features that are found in other membrane segments that move between the ER and the LDs[13], such as prolines at the centre of the motif (position 14 and 18 in the iMS of mouse PLIN1) as well as large hydrophobic residues like two internal tryptophanes (**Fig. S4G**). The iMS also contains positively charged residues but instead of being in the core of the motif (**Fig. S4G**)[13], they flank the iMS, perhaps ensuring the correct membrane topology of PLIN1 or contributing to the regulation of LD access. Consistent with *in vitro* studies[48] our data indicate that the iMS favours the LD surface over the ER bilayer. Its high LD affinity might even reflect the ability to directly bind TAGs, which would possibly explain why it is readily sequestered to the large LDs of adipocytes and its abundance in the ER is low. In early adipocytes PLIN1 likely reaches the LDs from the ER on the class-I route using physical connections between the ER and LDs called "bridges"[27,49]. In later adipocytes which contain larger LDs, access may depend on other pathways which were only recently identified[50]. Another possibility may involve a cytoplasmic intermediate (**Fig. S4F ER→cytoplasm→LD**) as proposed by others[44]. However,

unless this potential cytoplasmic form of PLIN1 is for an unknown reason quantitatively sedimenting to the alkaline resistant membrane fraction, our data seem to exclude this route.

Why the PLIN1 covered LD-class does not efficiently expand upon fatty acid feeding and a second LD-population is required to buffer rapid TAG synthesis, is currently unknown. PLIN1 is, however, essential for adipose tissue function and cannot be replaced by the other PLINs: Loss of PLIN1 function in mice and humans can cause lipodystrophy characterized by dysfunctional or absent white adipose tissue[4,51]. PLIN1 ablation in mice leads to increased basal adipose lipolysis preventing efficient build-up of LDs[52,53]. Complete loss of PLIN1 function in humans is metabolically detrimental rendering the affected patients insulin-resistant and often causes hypertriglyceridemia, cardiovascular problems and fatty liver disease[53,54]. Partial loss of PLIN1 or PLIN1 haploinsufficiency can, surprisingly, have beneficial effects on metabolic health[55]. According to recent reports some shorter PLIN1 truncation mutants in fact improve metabolic profiles and reduce risk for cardiovascular disease[56,57]. A controlled perturbation of PLIN1 membrane targeting might therefore open new avenues for mechanism-based therapy of fatty liver disease, type-2 diabetes, and obesity.

**Acknowledgements**

We thank Pedro Carvalho (University of Oxford) for critical reading of the manuscript and Lucas Pelkmans, University of Zurich, for generous support with research infrastructure.

A.R.T. was supported by **ANR-MOBIL** and **ANR-21-CE11-LIPRODYN**. R.W.K acknowledges support from the Swiss National Science Foundation (**SNF 31003A_159793**), the Helmut Horten Foundation, and E.P. Abraham Cephalosporin fund. This publication arises from research funded by the John Fell Oxford University Press Research Fund and a grant from Diabetes UK (**22/0006453)**. R.W.K. acknowledges support from the imaging facility at the Dunn School of Pathology, University of Oxford.

**Author contribution:**

**Conceptualization,** R.W.K; **Methodology,** M.M., R.W.K., A.R.T; **Formal analysis,** M.M., O.S., D.A., K.B., M.O, A.R.T, R.W.K.; **Investigation,** M.M., O.S., D.A., K.B., M.O, A.R.T, R.W.K.; **Resources,** A.R.T. and R.W.K; **Writing – Original draft ,** R.W.K.; **Writing – Review & Editing,** M.M., O.S., A.R.T., R.W.K., **Visualization;** M.M., O.S., A.R.T., R.W.K.; **Supervision,** A.R.T. and R.W.K.; **Funding Acquisition;** A.R.T and R.W.K.

**Declaration of Interests**

The authors declare no competing interests.

381 **References**
382
383
384 1. Rosen, E.D., and Spiegelman, B.M. (2006). Adipocytes as regulators of energy balance and
385 glucose homeostasis. Nature *444*, 847 853. 10.1038/nature05483.
386 2. Morigny, P., Boucher, J., Arner, P., and Langin, D. (2021). Lipid and glucose metabolism in
387 white adipocytes: pathways, dysfunction and therapeutics. Nat Rev Endocrinol *17*, 276–295.
388 10.1038/s41574-021-00471-8.
389 3. Grabner, G.F., Xie, H., Schweiger, M., and Zechner, R. (2021). Lipolysis: cellular mechanisms
390 for lipid mobilization from fat stores. Nat Metabolism *3*, 1445–1465. 10.1038/s42255-021-
391 00493-6.
392 4. Robbins, A.L., and Savage, D.B. (2015). The genetics of lipid storage and human
393 lipodystrophies. Trends Mol Med *21*, 1 6. 10.1016/j.molmed.2015.04.004.
394 5. Samuel, V.T., and Shulman, G.I. (2012). Mechanisms for Insulin Resistance: Common Threads
395 and Missing Links. Cell *148*, 852–871. 10.1016/j.cell.2012.02.017.
396 6. Guilherme, A., Virbasius, J.V., Puri, V., and Czech, M.P. (2008). Adipocyte dysfunctions linking
397 obesity to insulin resistance and type 2 diabetes. Nat Rev Mol Cell Bio *9*, 367 377.
398 10.1038/nrm2391.
399 7. Olzmann, J.A., and Carvalho, P. (2019). Dynamics and functions of lipid droplets. Nat Rev Mol
400 Cell Bio *20*, 137 155. 10.1038/s41580-018-0085-z.
401 8. Walther, T.C., Chung, J., and Farese, R.V. (2017). Lipid Droplet Biogenesis. Annu Rev Cell Dev
402 Bi *33*, 491–510. 10.1146/annurev-cellbio-100616-060608.
403 9. Pol, A., Gross, S.P., and Parton, R.G. (2014). Review: biogenesis of the multifunctional lipid
404 droplet: lipids, proteins, and sites. J Cell Biology *204*, 635 646. 10.1083/jcb.201311051.
405 10. Wolins, N.E., Quaynor, B.K., Skinner, J.R., Schoenfish, M.J., Tzekov, A., and Bickel, P.E.
406 (2005). S3-12, Adipophilin, and TIP47 package lipid in adipocytes. J Biol Chem *280*, 19146
407 19155. 10.1074/jbc.m500978200.
408 11. Wolins, N.E., Quaynor, B.K., Skinner, J.R., Tzekov, A., Croce, M.A., Gropler, M.C., Varma, V.,
409 Yao-Borengasser, A., Rasouli, N., Kern, P.A., et al. (2006). OXPAT/PAT-1 is a PPAR-induced lipid
410 droplet protein that promotes fatty acid utilization. Diabetes *55*, 3418 3428. 10.2337/db06-
411 0399.
412 12. Kassan, A., Herms, A., Fernández-Vidal, A., Bosch, M., Schieber, N.L., Reddy, B.J.N., Fajardo,
413 A., Gelabert-Baldrich, M., Tebar, F., Enrich, C., et al. (2013). Acyl-CoA synthetase 3 promotes
414 lipid droplet biogenesis in ER microdomains. J Cell Biology *203*, 985 1001.
415 10.1083/jcb.201305142.
416 13. Olarte, M.-J., Kim, S., Sharp, M.E., Swanson, J.M.J., Farese, R.V., and Walther, T.C. (2020).
417 Determinants of Endoplasmic Reticulum-to-Lipid Droplet Protein Targeting. Dev Cell.
418 10.1016/j.devcel.2020.07.001.
419 14. Dhiman, R., Caesar, S., Thiam, A.R., and Schrul, B. (2019). Mechanisms of protein targeting
420 to lipid droplets: A unified cell biological and biophysical perspective. Semin. cell Dev. Biol. *108*,
421 4–13. 10.1016/j.semcdb.2020.03.004.
422 15. Wilfling, F., Wang, H., Haas, J.T., Krahmer, N., Gould, T.J., Uchida, A., Cheng, J.-X., Graham,
423 M., Christiano, R., Fröhlich, F., et al. (2013). Triacylglycerol synthesis enzymes mediate lipid

424 droplet growth by relocalizing from the ER to lipid droplets. Dev Cell *24*, 384 399.
425 10.1016/j.devcel.2013.01.013.
426 16. Eisenberg-Bord, M., Mari, M., Weill, U., Rosenfeld-Gur, E., Moldavski, O., Castro, I.G., Soni,
427 K.G., Harpaz, N., Levine, T.P., Futerman, A.H., et al. (2018). Identification of seipin-linked factors
428 that act as determinants of a lipid droplet subpopulation. J Cell Biol *217*, 269 282.
429 10.1083/jcb.201704122.
430 17. Chitraju, C., Mejhert, N., Haas, J.T., Diaz-Ramirez, L.G., Grueter, C.A., Imbriglio, J.E., Pinto, S.,
431 Koliwad, S.K., Walther, T.C., and Jr, R.V.F. (2017). Triglyceride Synthesis by DGAT1 Protects
432 Adipocytes from Lipid-Induced ER Stress during Lipolysis. Cell Metab *26*, 407 418.e3.
433 10.1016/j.cmet.2017.07.012.
434 18. Thiam, A.R., and Beller, M. (2017). The why, when and how of lipid droplet diversity. J Cell
435 Sci *130*, 315–324. 10.1242/jcs.192021.
436 19. Straub, B.K., Stoeffel, P., Heid, H., Zimbelmann, R., and Schirmacher, P. (2008). Differential
437 pattern of lipid droplet-associated proteins and de novo perilipin expression in hepatocyte
438 steatogenesis. Hepatology *47*, 1936–1946. 10.1002/hep.22268.
439 20. Hsieh, K., Lee, Y.K., Londos, C., Raaka, B.M., Dalen, K.T., and Kimmel, A.R. (2012). Perilipin
440 family members preferentially sequester to either triacylglycerol-specific or cholesteryl-ester-
441 specific intracellular lipid storage droplets. J Cell Sci *125*, 4067 4076. 10.1242/jcs.104943.
442 21. Herms, A., Bosch, M., Ariotti, N., Reddy, B.J.N., Fajardo, A., Fernández-Vidal, A., Alvarez-
443 Guaita, A., Fernández-Rojo, M.A., Rentero, C., Tebar, F., et al. (2013). Cell-to-cell heterogeneity
444 in lipid droplets suggests a mechanism to reduce lipotoxicity. Curr Biol *23*, 1489 1496.
445 10.1016/j.cub.2013.06.032.
446 22. Henne, M., Goodman, J.M., and Hariri, H. (2019). Spatial compartmentalization of lipid
447 droplet biogenesis. Biochimica Et Biophysica Acta Mol Cell Biology Lipids *1865*, 158499.
448 10.1016/j.bbalip.2019.07.008.
449 23. Ugrankar, R., Bowerman, J., Hariri, H., Chandra, M., Chen, K., Bossanyi, M.-F., Datta, S.,
450 Rogers, S., Eckert, K.M., Vale, G., et al. (2019). Drosophila Snazarus Regulates a Lipid Droplet
451 Population at Plasma Membrane-Droplet Contacts in Adipocytes. Dev Cell *50*, 557-572.e5.
452 10.1016/j.devcel.2019.07.021.
453 24. Heid, H., Rickelt, S., Zimbelmann, R., Winter, S., Schumacher, H., Dörflinger, Y., Kuhn, C., and
454 Franke, W.W. (2014). On the formation of lipid droplets in human adipocytes: the organization
455 of the perilipin-vimentin cortex. Plos One *9*, e90386. 10.1371/journal.pone.0090386.
456 25. Wolins, N.E., Brasaemle, D.L., and Bickel, P.E. (2006). A proposed model of fat packaging by
457 exchangeable lipid droplet proteins. Febs Lett *580*, 5484 5491. 10.1016/j.febslet.2006.08.040.
458 26. Freyre, C.A.C., Rauher, P.C., Ejsing, C.S., and Klemm, R.W. (2019). MIGA2 Links
459 Mitochondria, the ER, and Lipid Droplets and Promotes De Novo Lipogenesis in Adipocytes. Mol
460 Cell *76*, 811-825.e14. 10.1016/j.molcel.2019.09.011.
461 27. Kory, N., Farese, R.V., and Walther, T.C. (2016). Targeting Fat: Mechanisms of Protein
462 Localization to Lipid Droplets. Trends Cell Biol *26*. 10.1016/j.tcb.2016.02.007.
463 28. Olarte, M.-J., Swanson, J.M.J., Walther, T.C., and Farese, R.V. (2022). The CYTOLD and
464 ERTOLD pathways for lipid droplet–protein targeting. Trends Biochem. Sci. *47*, 39–51.
465 10.1016/j.tibs.2021.08.007.

466 29. Prévost, C., Sharp, M.E., Kory, N., Lin, Q., Voth, G.A., Farese, R.V., and Walther, T.C. (2018).
467 Mechanism and Determinants of Amphipathic Helix-Containing Protein Targeting to Lipid
468 Droplets. Dev Cell *44*, 73 86.e4. 10.1016/j.devcel.2017.12.011.
469 30. Kory, N., Thiam, A.-R., Farese, R.V., and Walther, T.C. (2015). Protein Crowding Is a
470 Determinant of Lipid Droplet Protein Composition. Dev Cell *34*, 351–363.
471 10.1016/j.devcel.2015.06.007.
472 31. Rowe, E.R., Mimmack, M.L., Barbosa, A.D., Haider, A., Isaac, I., Ouberai, M.M., Thiam, A.R.,
473 Patel, S., Saudek, V., Siniossoglou, S., et al. (2016). Conserved Amphipathic Helices Mediate
474 Lipid Droplet Targeting of Perilipins 1-3. J Biol Chem *291*, 6664 6678. 10.1074/jbc.m115.691048.
475 32. Čopič, A., Antoine-Bally, S., Giménez-Andrés, M., Garay, C.T., Antonny, B., Manni, M.M.,
476 Pagnotta, S., Guihot, J., and Jackson, C.L. (2018). A giant amphipathic helix from a perilipin that
477 is adapted for coating lipid droplets. Nat Commun *9*, 1 16. 10.1038/s41467-018-03717-8.
478 33. Giménez-Andrés, M., Emeršič, T., Antoine-Bally, S., D'Ambrosio, J.M., Antonny, B., Derganc,
479 J., and Čopič, A. (2021). Exceptional stability of a perilipin on lipid droplets depends on its polar
480 residues, suggesting multimeric assembly. Elife *10*, e61401. 10.7554/elife.61401.
481 34. Chorlay, A., Monticelli, L., Ferreira, J.V., M'barek, K.B., Ajjaji, D., Wang, S., Johnson, E., Beck,
482 R., Omrane, M., Beller, M., et al. (2019). Membrane Asymmetry Imposes Directionality on Lipid
483 Droplet Emergence from the ER. Dev Cell *50*, 25-42.e7. 10.1016/j.devcel.2019.05.003.
484 35. Bickel, P.E., Tansey, J.T., and Welte, M.A. (2009). PAT proteins, an ancient family of lipid
485 droplet proteins that regulate cellular lipid stores. Biochimica Et Biophysica Acta Bba - Mol Cell
486 Biology Lipids *1791*, 419 440. 10.1016/j.bbalip.2009.04.002.
487 36. Londos, C., Brasaemle, D.L., Schultz, C.J., Segrest, J.P., and Kimmel, A.R. (1999). Perilipins,
488 ADRP, and other proteins that associate with intracellular neutral lipid droplets in animal cells.
489 Semin Cell Dev Biol *10*, 51 58. 10.1006/scdb.1998.0275.
490 37. Kimmel, A.R., and Sztalryd, C. (2016). The Perilipins: Major Cytosolic Lipid Droplet–
491 Associated Proteins and Their Roles in Cellular Lipid Storage, Mobilization, and Systemic
492 Homeostasis*. Annu Rev Nutr *36*, 471 509. 10.1146/annurev-nutr-071813-105410.
493 38. Brasaemle, D.L. (2007). Thematic review series: adipocyte biology. The perilipin family of
494 structural lipid droplet proteins: stabilization of lipid droplets and control of lipolysis. J Lipid Res
495 *48*, 2547 2559. 10.1194/jlr.r700014-jlr200.
496 39. Garcia, A., Subramanian, V., Sekowski, A., Bhattacharyya, S., Love, M.W., and Brasaemle,
497 D.L. (2004). The amino and carboxyl termini of perilipin a facilitate the storage of
498 triacylglycerols. J Biol Chem *279*, 8409 8416. 10.1074/jbc.m311198200.
499 40. Choi, Y.M., Ajjaji, D., Fleming, K.D., Borbat, P.P., Jenkins, M.L., Moeller, B.E., Fernando, S.,
500 Bhatia, S.R., Freed, J.H., Burke, J.E., et al. (2023). Structural insights into perilipin 3 membrane
501 association in response to diacylglycerol accumulation. Nat. Commun. *14*, 3204.
502 10.1038/s41467-023-38725-w.
503 41. Garcia, A., Sekowski, A., Subramanian, V., and Brasaemle, D.L. (2003). The central domain is
504 required to target and anchor perilipin A to lipid droplets. J Biol Chem *278*, 625 635.
505 10.1074/jbc.m206602200.
506 42. Ajjaji, D., M'barek, K.B., Mimmack, M.L., England, C., Herscovitz, H., Dong, L., Kay, R.G.,
507 Patel, S., Saudek, V., Small, D.M., et al. (2019). Dual binding motifs underpin the hierarchical
508 association of perilipins1–3 with lipid droplets. Mol Biol Cell *30*, 703–716. 10.1091/mbc.e18-08-
509 0534.

510 43. Wolins, N.E., Skinner, J.R., Schoenfish, M.J., Tzekov, A., Bensch, K.G., and Bickel, P.E. (2003).
511 Adipocyte protein S3-12 coats nascent lipid droplets. J Biol Chem *278*, 37713 37721.
512 10.1074/jbc.m304025200.
513 44. Skinner, J.R., Harris, L.-A.L.S., Shew, T.M., Abumrad, N.A., and Wolins, N.E. (2013). Perilipin 1
514 moves between the fat droplet and the endoplasmic reticulum. Adipocyte *2*, 80 86.
515 10.4161/adip.22864.
516 45. Shibata, Y., Hu, J., Kozlov, M.M., and Rapoport, T.A. (2009). Mechanisms shaping the
517 membranes of cellular organelles. Annu Rev Cell Dev Bi *25*, 329 354.
518 10.1146/annurev.cellbio.042308.113324.
519 46. Parton, R.G., and Pozo, M.A. del (2013). Caveolae as plasma membrane sensors, protectors
520 and organizers. Nat Rev Mol Cell Bio *14*, 98 112. 10.1038/nrm3512.
521 47. Schrul, B., and Kopito, R.R. (2016). Peroxin-dependent targeting of a lipid-droplet-destined
522 membrane protein to ER subdomains. Nat Cell Biol *18*, 1 26. 10.1038/ncb3373.
523 48. Caillon, L., Nieto, V., Gehan, P., Omrane, M., Rodriguez, N., Monticelli, L., and Thiam, A.R.
524 (2020). Triacylglycerols sequester monotopic membrane proteins to lipid droplets. Nat
525 Commun *11*, 3944. 10.1038/s41467-020-17585-8.
526 49. Wilfling, F., Thiam, A.R., Olarte, M.-J., Wang, J., Beck, R., Gould, T.J., Allgeyer, E.S., Pincet, F.,
527 Bewersdorf, J., Farese, R.V., et al. (2014). Arf1/COPI machinery acts directly on lipid droplets
528 and enables their connection to the ER for protein targeting. Elife *3*, e01607.
529 10.7554/elife.01607.
530 50. Song, J., Mizrak, A., Lee, C.-W., Cicconet, M., Lai, Z.W., Tang, W.-C., Lu, C.-H., Mohr, S.E.,
531 Farese, R.V., and Walther, T.C. (2022). Identification of two pathways mediating protein
532 targeting from ER to lipid droplets. Nat Cell Biol, 1–14. 10.1038/s41556-022-00974-0.
533 51. Mann, J.P., and Savage, D.B. (2019). What lipodystrophies teach us about the metabolic
534 syndrome. J Clin Invest *129*, 4009–4021. 10.1172/jci129190.
535 52. Tansey, J.T., Sztalryd, C., Gruia-Gray, J., Roush, D.L., Zee, J.V., Gavrilova, O., Reitman, M.L.,
536 Deng, C.-X., Li, C., Kimmel, A.R., et al. (2001). Perilipin ablation results in a lean mouse with
537 aberrant adipocyte lipolysis, enhanced leptin production, and resistance to diet-induced
538 obesity. Proc. Natl. Acad. Sci. *98*, 6494–6499. 10.1073/pnas.101042998.
539 53. Gandotra, S., Lim, K., Girousse, A., Saudek, V., O'Rahilly, S., and Savage, D.B. (2011). Human
540 frame shift mutations affecting the carboxyl terminus of perilipin increase lipolysis by failing to
541 sequester the adipose triglyceride lipase (ATGL) coactivator AB-hydrolase-containing 5
542 (ABHD5). J Biological Chem *286*, 34998–35006. 10.1074/jbc.m111.278853.
543 54. Garg, A. (2011). Clinical review#: Lipodystrophies: genetic and acquired body fat disorders. J
544 Clin Endocrinol Metabolism *96*, 3313 3325. 10.1210/jc.2011-1159.
545 55. Melvin, A., Stears, A., and Savage, D.B. (2019). Recent developments in lipodystrophy. Curr.
546 Opin. Lipidol. *30*, 284–290. 10.1097/mol.0000000000000613.
547 56. Koprulu, M., Zhao, Y., Wheeler, E., Dong, L., Rocha, N., Li, C., Griffin, J.D., Patel, S., Streek,
548 M.V. de, Glastonbury, C.A., et al. (2021). Identification of rare loss of function genetic variation
549 regulating body fat distribution. J. Clin. Endocrinol. Metab. *107*, dgab877-.
550 10.1210/clinem/dgab877.
551 57. Patel, K.A., Burman, S., Laver, T.W., Hattersley, A.T., Frayling, T.M., and Weedon, M.N.
552 (2022). PLIN1 Haploinsufficiency Causes a Favorable Metabolic Profile. J. Clin. Endocrinol.
553 Metab. *107*, e2318–e2323. 10.1210/clinem/dgac104.

554 58. Krogh, A., Larsson, B., Heijne, G. von, and Sonnhammer, E.L. (2001). Predicting
555 transmembrane protein topology with a hidden Markov model: application to complete
556 genomes. J Mol Biol *305*, 567 580. 10.1006/jmbi.2000.4315.
557 59. Jayasinghe, S., Hristova, K., and White, S.H. (2001). Energetics, stability, and prediction of
558 transmembrane helices. J Mol Biol *312*, 927 934. 10.1006/jmbi.2001.5008.
559

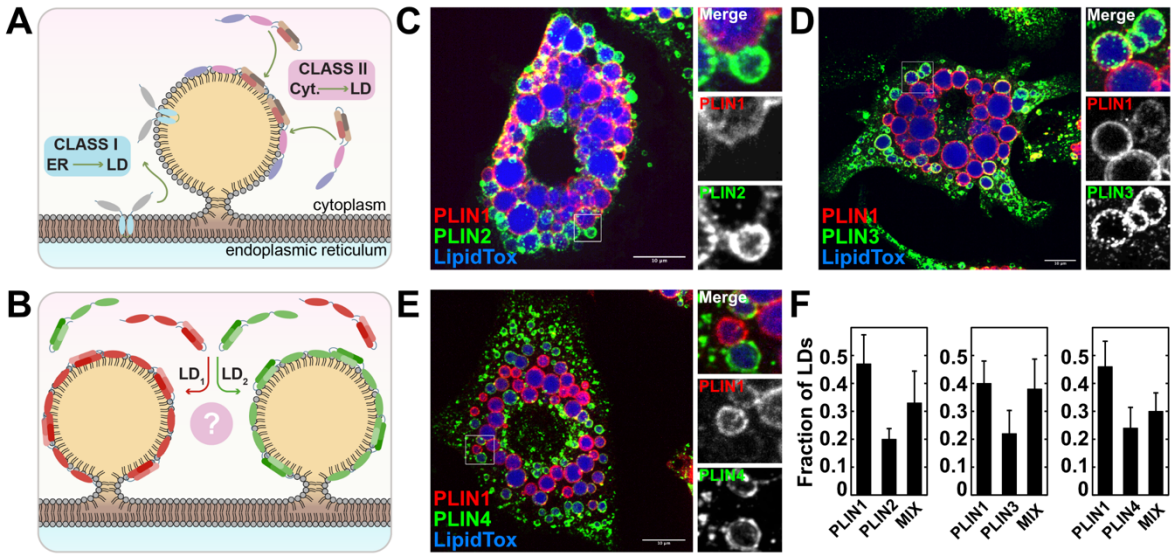
A
CLASS II
Cyt. → LD
CLASS I
ER → LD
cytoplasm
endoplasmic reticulum
B
LD1
LD2
?
C
Merge
PLIN1
PLIN2
LipidTox
D
Merge
PLIN1
PLIN3
LipidTox
E
Merge
PLIN1
PLIN4
LipidTox
F
Fraction of LDs
0.5
0.4
0.3
0.2
0.1
0
PLIN1
PLIN2
MIX
PLIN1
PLIN3
MIX
PLIN1
PLIN4
MIX

**Figure 1**

560

561 **Figure 1**
562 **Fatty acid feeding leads to the formation of at least two distinct LD-classes in adipocytes.**
563 **(A)** Class-I LD proteins are monotopic membrane proteins that move from the ER (membrane
564 brown, ER lumen blue) to the LD surface. Class-II LD proteins bind to LDs directly from the
565 cytoplasm (pink).
566 **(B)** Segregation of class-II proteins (e.g. perilipins) to different LD-classes.
567 **(C)** Day 6 3T3-L1 derived adipocytes were fed for 3h with 750 µM $Na^{2+}$oleate. Endogenously
568 expressed PLIN1 and PLIN2 were visualized by immunofluorescence. Scale bar, 10 µm.
569 **(D)** As in (C) but PLIN1 and PLIN3 were visualized.
570 **(E)** As in (C) but PLIN1 and PLIN4 were visualized.
571 **(F)** Quantification of the results in (C)-(E). n=9; n=9; n=8, for cells co-stained with PLIN1 and 2 or
572 PLIN1 and 3 or PLIN1 and 4, respectively. LD counts per replicate >100; values are expressed as
573 mean LD in each class ± SEM.
574

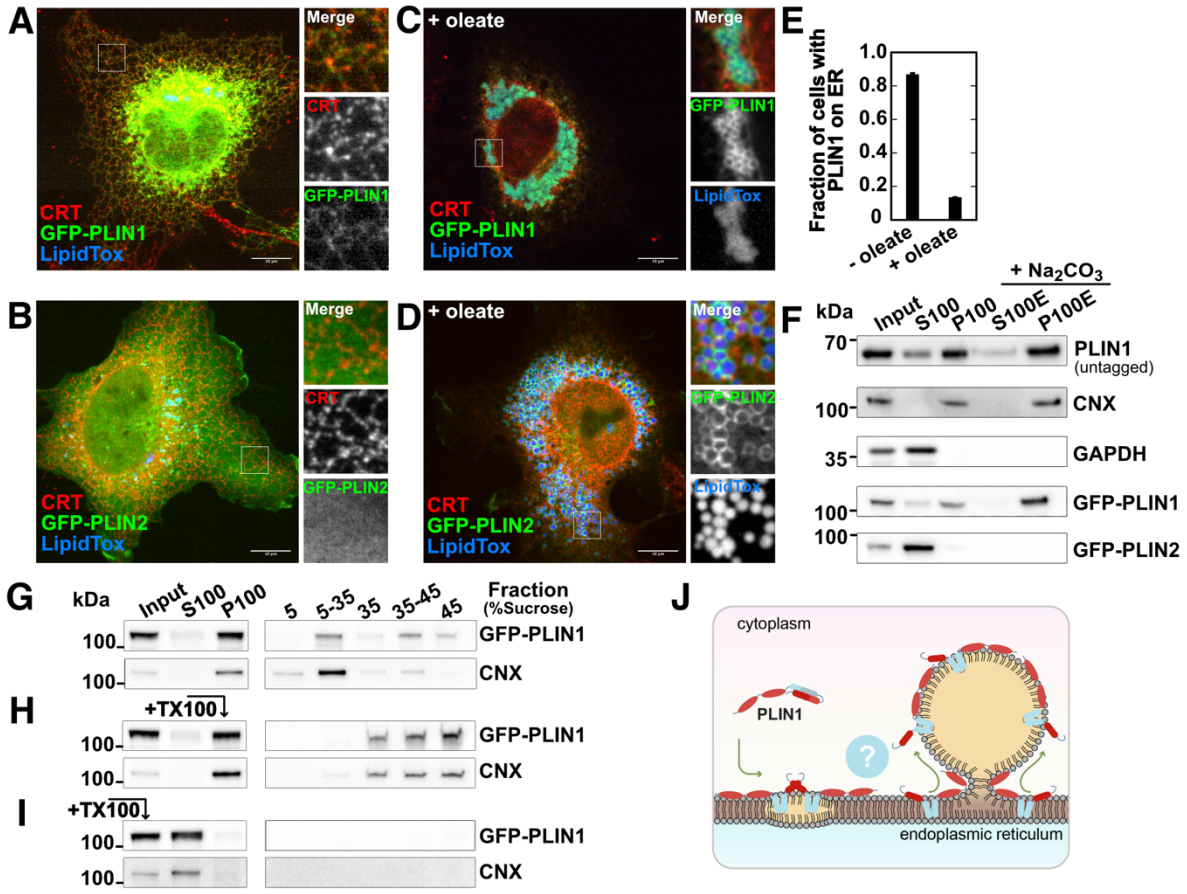
A
Merge
CRT
GFP-PLIN1
CRT
GFP-PLIN1
LipidTox
C
+ oleate
Merge
GFP-PLIN1
LipidTox
CRT
GFP-PLIN1
LipidTox
E
Fraction of cells with PLIN1 on ER
1.0
0.8
0.6
0.4
0.2
0
- oleate
+ oleate
B
Merge
CRT
GFP-PLIN2
CRT
GFP-PLIN2
LipidTox
D
+ oleate
Merge
GFP-PLIN2
LipidTox
CRT
GFP-PLIN2
LipidTox
F
+ Na2CO3
kDa
Input
S100
P100
S100E
P100E
70
PLIN1
(untagged)
100
CNX
35
GAPDH
100
GFP-PLIN1
100
GFP-PLIN2
G
kDa
Input
S100
P100
5
5-35
35
35-45
45
Fraction
(%Sucrose)
100
GFP-PLIN1
100
CNX
H
+TX100
100
GFP-PLIN1
100
CNX
I
+TX100
100
GFP-PLIN1
100
CNX
J
cytoplasm
PLIN1
?
endoplasmic reticulum

**Figure 2**

575

576 **Figure 2**
577 **PLIN1 is an integral membrane protein which localizes to the ER and LDs.**
578 **(A)** Mouse PLIN1 tagged at its N-terminus with GFP (GFP-PLIN1) was expressed in COS7 cells.
579 The ER is visualized with an antibody specific to the luminal ER protein calreticulin (CRT). LDs
580 are stained with LipidToxRed. Scale bar, 10 µm.
581 **(B)** As in (A) but the cells were transfected with GFP-PLIN2.
582 **(C)** As in (A) but 250 µM $Na^+$oleate was added for 6h prior to fixation.
583 **(D)** As in (C) but the cells were transfected with GFP-PLIN2.
584 **(E)** Quantification of results in (A) and (C) using supervised machine learning to identify cells
585 with GFP-PLIN1 on the ER. n = 3 independent experiments with >1500 cell per replicate; values
586 are expressed as the mean fraction of cells with PLIN1 on the ER ±SD.
587 **(F)** COS7 cells were transfected with untagged PLIN1, GFP-PLIN1 or GFP-PLIN2, and subjected to
588 fractionation followed by alkaline extraction. **Input,** cell lysate; **S100, P100,** supernatant and
589 pellet of a 100k x g centrifugation step, **S100E, P100E,** supernatant and pellet of 100k x g
590 centrifugation after alkaline extraction with $Na_2CO_3$. **GAPDH,** glycerolaldehyde-3-phosphate
591 dehydrogenase (cytoplasm); **CNX,** calnexin (integral ER-membrane protein).
592 **(G)** As in (F), but P100 was subjected to flotation on a sucrose step gradient with the indicated
593 concentrations.
594 **(H)** As in (G), but P100 was incubated with Triton X-100 before flotation.
595 **(I)** As in (H), but the cell lysate (input) was treated with Triton X-100 before centrifugation at
596 100k x g.
597 **(J)** PLIN1 is an integral membrane protein with a membrane anchor (blue) allowing dual
598 targeting to the ER and the LD surface (unknown pathway indicated as “?”).
599

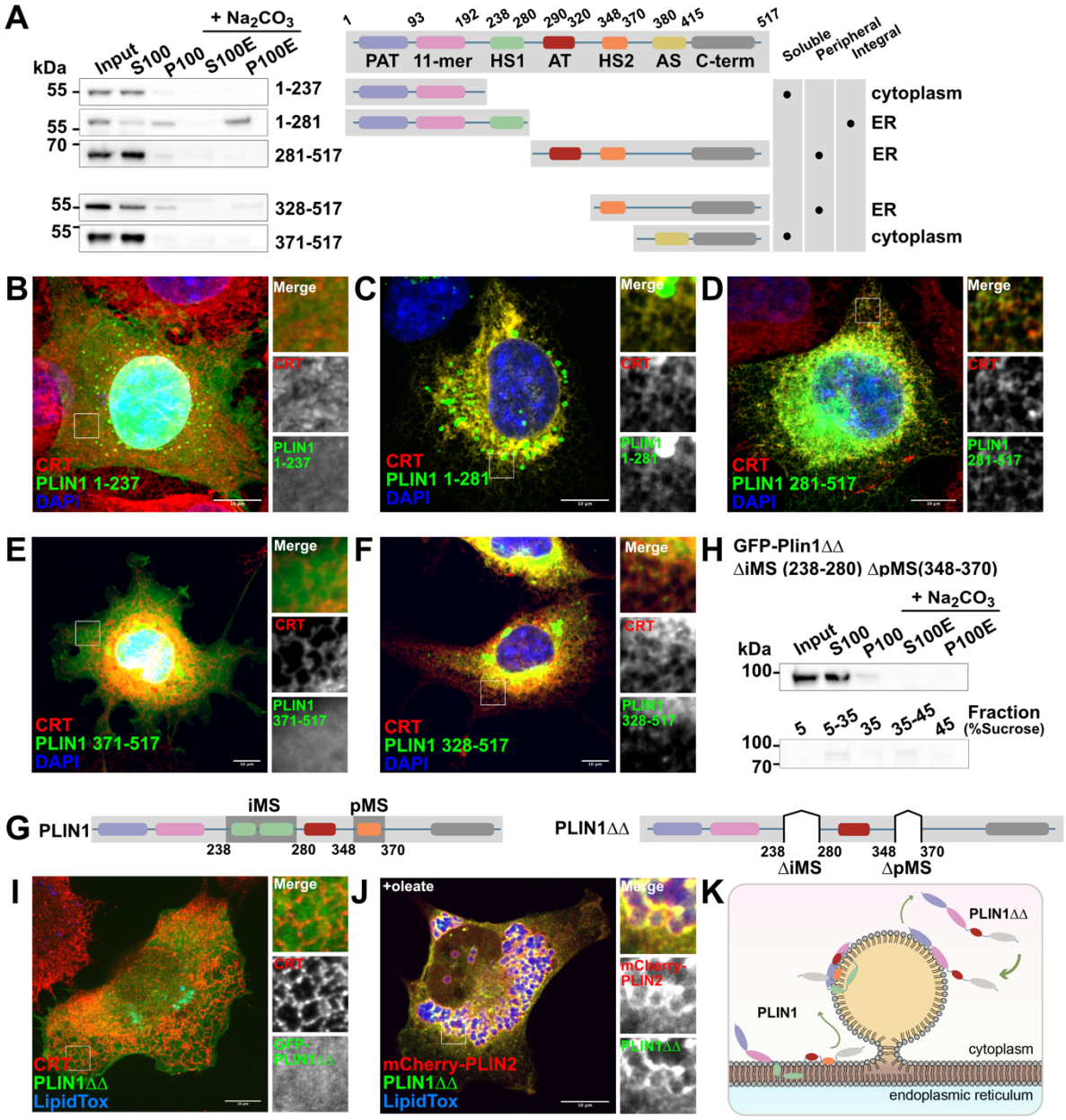
A
+ Na2CO3
kDa
Input
S100
P100
S100E
P100E
55
55
70
55
55
1-237
1-281
281-517
328-517
371-517
1
93
192
238
280
290
320
348
370
380
415
517
PAT
11-mer
HS1
AT
HS2
AS
C-term
Soluble
Peripheral
Integral
cytoplasm
ER
ER
ER
cytoplasm
B
Merge
CRT
PLIN1 1-237
DAPI
C
CRT
PLIN1 1-281
DAPI
D
CRT
PLIN1 281-517
DAPI
E
CRT
PLIN1 371-517
DAPI
F
CRT
PLIN1 328-517
DAPI
H
GFP-Plin1ΔΔ
ΔiMS (238-280) ΔpMS(348-370)
+ Na2CO3
kDa
Input
S100
P100
S100E
P100E
100
100
70
5
5-35
35
35-45
45
Fraction
(%Sucrose)
G
PLIN1
iMS
pMS
238
280
348
370
PLIN1ΔΔ
238
280
348
370
ΔiMS
ΔpMS
I
CRT
PLIN1ΔΔ
LipidTox
J
+oleate
mCherry-PLIN2
PLIN1ΔΔ
LipidTox
K
PLIN1ΔΔ
PLIN1
cytoplasm
endoplasmic reticulum

**Figure 3**

600

601 **Figure 3**
602 **Identification of two ER targeting segments in PLIN1.**
603 **(A)** Structure-function analysis of PLIN1 by fractionation and alkaline extraction using the
604 indicated truncation constructs and immune-blotting with a anti GFP-antibody.
605 **PAT,** perilipin, adipohilin/ADRP, TIP-47 domain (purple); **11-mer,** LD targeting region (pink);
606 **HS1, 2** hydrophobic segment 1 and 2 (green, orange, resp.); **AT,** acidic tract (red); **AS,**
607 amphipathic segment (yellow); **C-term,** carboxy terminus with regulatory elements (grey).
608 Classification explained in Fig. S3B.
609 **(B)** COS7 cells expressing a GFP-tagged N-terminal portion of PLIN1 (1-237). The ER was
610 visualized by immunofluorescence with an antibody to calreticulin (CRT). The nuclei were
611 stained with DAPI. Scale bar, 10 µm.
612 **(C)** As in (B) but with a different truncation construct (PLIN1 1-281).
613 **(D)** As in (B) but with cells expressing the C-terminal truncation construct PLIN1 281-519.
614 **(E)** As in (D) but with PLIN1 371-517.
615 **(F)** As in (D) but with PLIN1 328-517.
616 **(G)** Same illustrations as in (A) but the integral membrane segment (iMS, 238-280) and the
617 peripheral membrane segment (pMS, 348-370) are highlighted. PLIN1ΔΔ lacks the iMS and the
618 pMS.
619 **(H)** As in (A) but with a construct lacking the iMS and the pMS (GFP-PLIN1ΔΔ). Membranes in the
620 P100 fraction were in parallel subjected to alkaline extraction (+$Na_2CO_3$) and flotation
621 experiments.
622 **(I)** As in (B) but with PLIN1ΔΔ and the LDs were stained with LipidToxDeepRed.
623 **(J)** COS7 cells were co-transfected with PLIN2 N-terminally tagged with mCherry2, and GFP
624 tagged PLIN1ΔΔ. The cells were treated with 250 µM $Na^+$oleate 6h prior to fixation.
625 **(K)** Deletion of the iMS and pMS results in a switch of LD-protein class with PLIN1 and PLIN1ΔΔ
626 behaving as class-I and class-II LD proteins, respectively. Domain description as in (A).
627

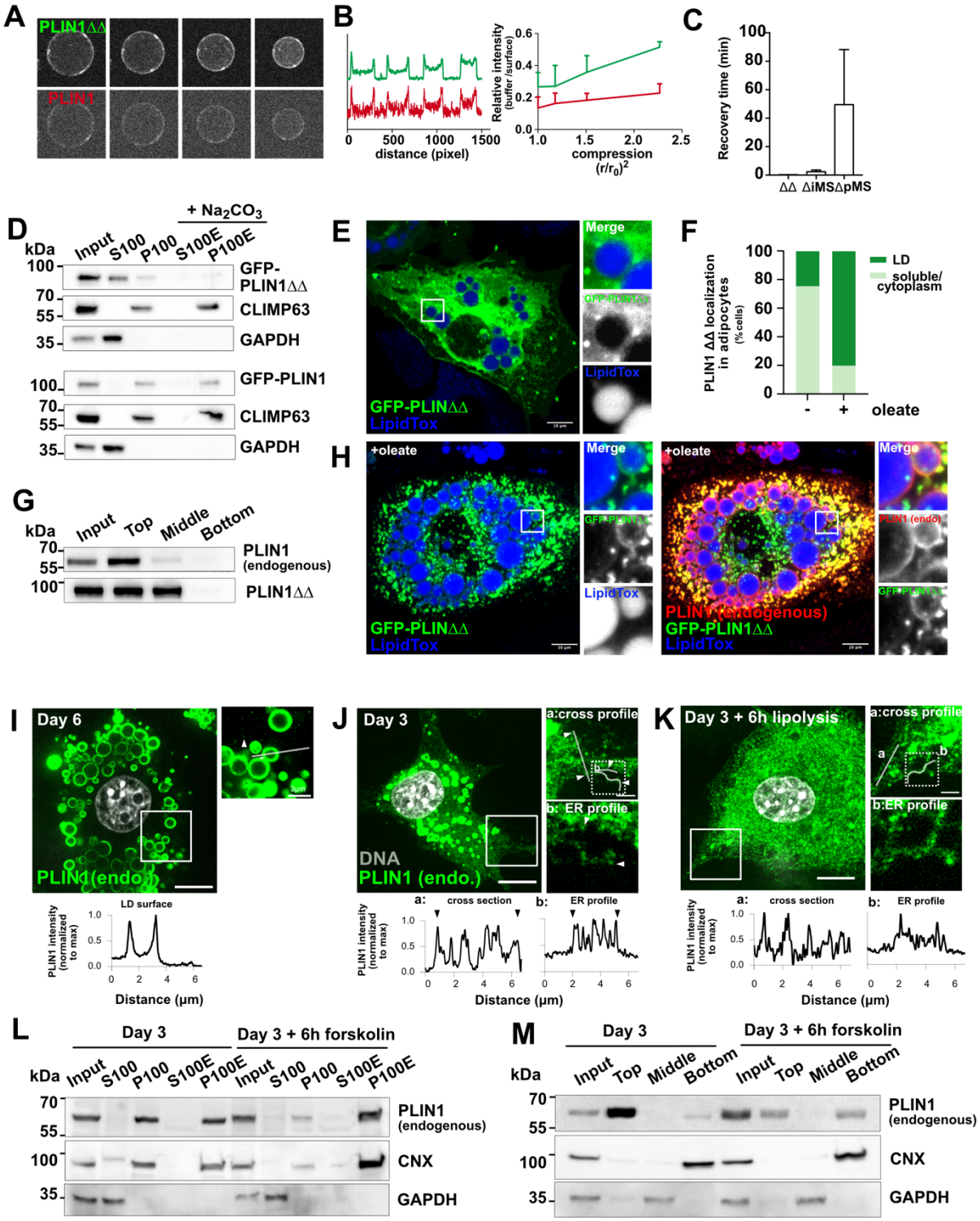
A
PLIN1ΔΔ
PLIN1
B
distance (pixel)
Relative intensity (buffer /surface)
compression (r/r0)2
C
Recovery time (min)
ΔΔ
ΔiMS
ΔpMS
D
+ Na2CO3
kDa
Input
S100
P100
S100E
P100E
GFP-PLIN1ΔΔ
CLIMP63
GAPDH
GFP-PLIN1
E
Merge
GFP-PLIN1ΔΔ
LipidTox
F
PLIN1 ΔΔ localization in adipocytes (% cells)
LD
soluble/ cytoplasm
oleate
G
Input
Top
Middle
Bottom
PLIN1 (endogenous)
PLIN1ΔΔ
H
+oleate
Merge
GFP-PLIN1ΔΔ
LipidTox
PLIN1 (endo)
PLIN1 (endogenous)
I
Day 6
PLIN1(endo)
LD surface
PLIN1 intensity (normalized to max)
Distance (µm)
J
Day 3
DNA
PLIN1 (endo.)
a:cross profile
b: ER profile
a: cross section
b: ER profile
K
Day 3 + 6h lipolysis
L
Day 3
Day 3 + 6h forskolin
CNX
M

**Figure 4**

628

629 **Figure 4**
630 **Membrane association determines LD-class specificity by tuning LD binding kinetics**
631 **(A)** GFP-PLIN1ΔΔ and mCherry-PLIN1 full-length were reconstituted in an buffer-in oil system
632 and their localization was monitored by microscopy as the aqueous phase progressively shrinks.
633 **(B)** Ratio of fluorescence intensity at the oil-buffer interface and in the buffer phase at 4
634 different surface compression ratios for PLIN1ΔΔ (green) and PLIN1 full length (red). N=3
635 independent experiments; mean ± SD.
636 **(C)** Fluorescence recovery after photobleaching in oleate treated Huh7 cells expressing GFP-
637 PLIN1ΔΔ, ΔiMS or ΔpMS. Scale bar, 10 µm. N = 3; results are expressed as mean ± SD.
638 **(D)** GFP-PLIN1ΔΔ or GFP-PLIN1 (full-length) were expressed in 3T3-L1 cells from a stably
639 integrated inducible transgene and subjected to fractionation and alkaline extraction. **Input,**
640 cell lysate; **S100, P100,** supernatant and pellet of a 100k x g centrifugation step, **S100E, P100E,**
641 supernatant and pellet of 100k x g centrifugation after alkaline extraction with 100 mM $Na_2CO_3$.
642 **GAPDH,** glyceraldehyde-3-phosphate dehydrogenase (cytoplasm); **CLIMP-63,** integral ER-
643 membrane protein.
644 **(E)** As in (D) but the cells were differentiated into adipocytes and expression of PLIN1ΔΔ was
645 induced 6 days post differentiation by the addition of 500 ng/ml anhydrotetracycline 6h prior to
646 fixation. LDs were stained with LipidToxDeepRed and visualized together with GFP-PLIN1ΔΔ by
647 fluorescence microscopy. Scale bar, 10 µm.
648 (**F**) Percentage of the cells in (E) and (H) in which GFP-PLIN1ΔΔ is either on peripheral LDs or in
649 the cytoplasm, N = 100 cells per group.
650 **(G)** As in (E) but the adipocytes were subjected to flotation. Endogenously expressed PLIN1 and
651 PLIN1ΔΔ were visualized by immuno-blotting with antibodies specific to the C-term of PLIN1
652 recognizing both proteins.
653 **(H)** As in (E) with addition of oleate 6h before fixation. In contrast to (F) GFP-PLIN1ΔΔ is now
654 found on peripheral LDs. PLIN1ΔΔ remains excluded from the central LDs covered by endogenous
655 PLIN1. On the right, additional staining with anti-PLIN1 antibody (red) recognizing both
656 endogenous PLIN1 on large LDs (red) and the PLIN1ΔΔ mutant on the peripheral LDs
657 (GFP+red=yellow).
658 (**I)** Localization of endogenous PLIN1 (green) in 3T3-L1 adipocytes at day 6 post differentiation;
659 line plot of PLIN1 intensity (normalized to maximum), as drawn in the inset.. Scale bar: 10 µm for
660 whole cell image, 4 m for inset 4 µm.
661 (J) As in (I), but at day 3 post differentiation endogenous PLIN1 is on the ER. Arrowheads mark
662 terminal points of ER network
663 (K) As in (J), but after addition of 10 µM forskolin to stimulate lipolysis for 6h prior to fixation.
664 (L) Fractionation and alkaline extraction of adipocytes as in (J) and (K); labels as in (D); **CNX**,
665 calnexin (integral ER-membrane protein).
666 (M) Flotation experiment of the cells as in (J) and (K), done as in (G).

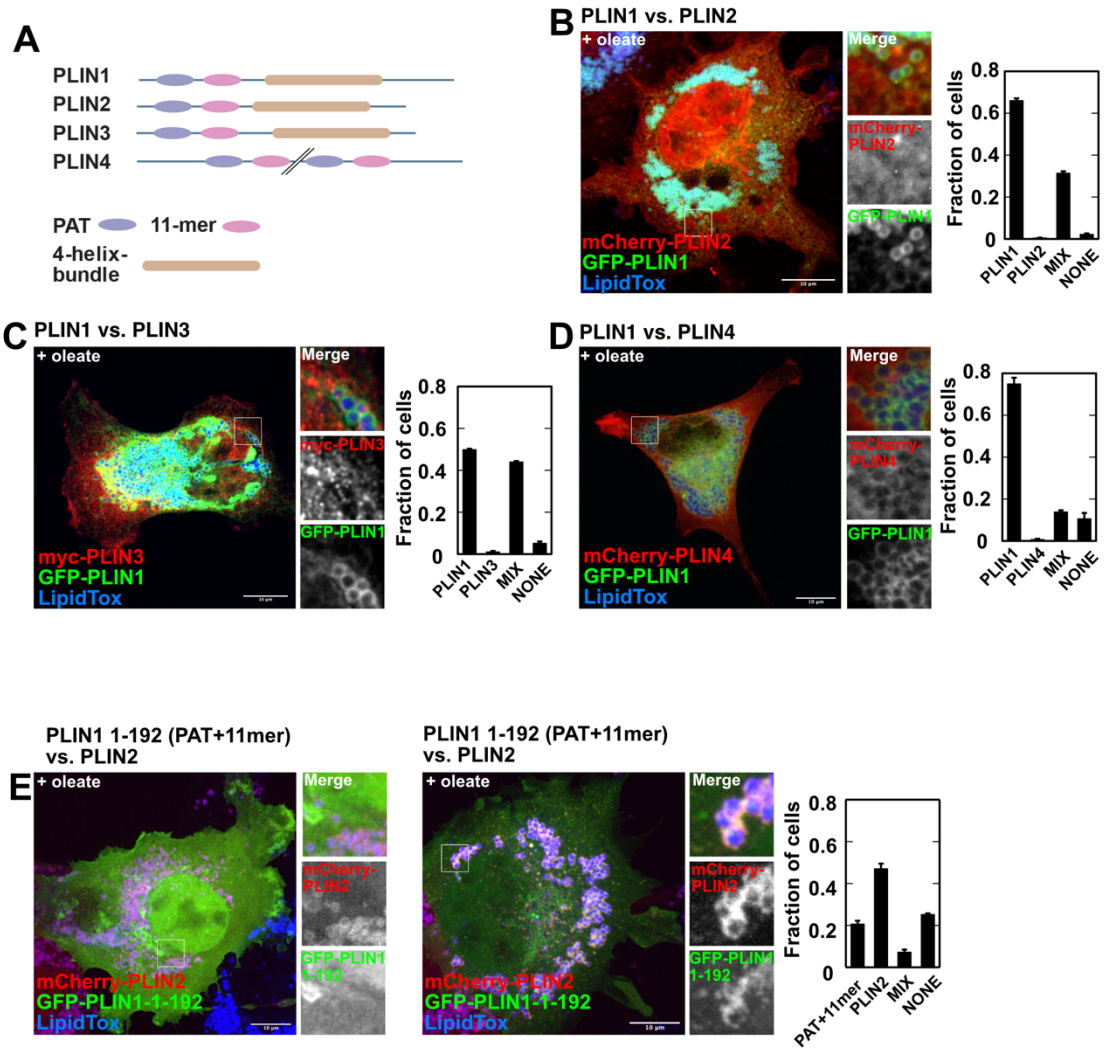


**Figure S1**

667

668 **Figure S1**
669 **PLIN1 excludes PLIN2, 3 and 4 from LD binding in COS7 cells.**
670 **(A)** Schematic representation of perilipin (PLIN) 1-4. The amino terminal PAT (perilipin,
671 adipophilin/ADRP domain) and 11-mer regions are important for LD targeting. PLIN1-3 contain a
672 predicted four helix bundle. The PLINs were grouped into a protein family based on the sequence
673 similarity found in the PAT and 11-mer domains as well as their localization to the LD surface.
674 PLIN4 does not contain a four-helix bundle and is much larger than the other family members.
675 **(B)** COS7 cells co-expressing PLIN1 tagged at its N-terminus with GFP (GFP-PLIN1) and PLIN2
676 carrying an N-terminal mCherry2 tag (mCherry-PLIN2). 250 µM $Na^+$oleate was added to the
677 growth medium 6h prior to fixation. Lipid droplets were stained with LipidToxDeepRed (LipidTox).
678 The cells were automatically segmented and assigned by a support vector machine based
679 classifier into 4 groups, in which PLIN1 was exclusively found on the LD surface and PLIN2 was
680 cytoplasmic **(PLIN1)**, cells that showed only PLIN2 LD staining **(PLIN2)**, cells in which various levels
681 of PLIN2 was found on LDs together with PLIN1 **(MIX)**, and cells in which neither of the two
682 proteins was found on the LD **(NONE)**. Intensity and texture of PLIN1 and PLIN2 channels as well
683 as correlation with LipidTOXDeepRed were used as training features. n = 3 independent
684 experiments ; the results are expressed as mean ±SD. Scale bar, 10µm.
685 **(C)** As in (B) but PLIN3 tagged at its N-terminus with c-myc (myc-PLIN3) was co-expressed with
686 GFP-PLIN1. n = 3 independent experiments ; the results are expressed as mean ±SD.
687 **(D)** As in (C) but PLIN4 tagged at its N-terminus with mCherry2 (mCherry-PLIN4) was co-expressed
688 with GFP-PLIN1. n = 3 independent experiments ; the results are expressed as mean ±SD.
689 **(E)** COS7 cells co-expressing PLIN1 truncated after the 11-mer at residue 192 tagged at its N-
690 terminus with a GFP (GFP-PLIN1-1-192) and PLIN2 tagged at its N-terminus with mCherry2
691 (mCherry-PLIN2).
692

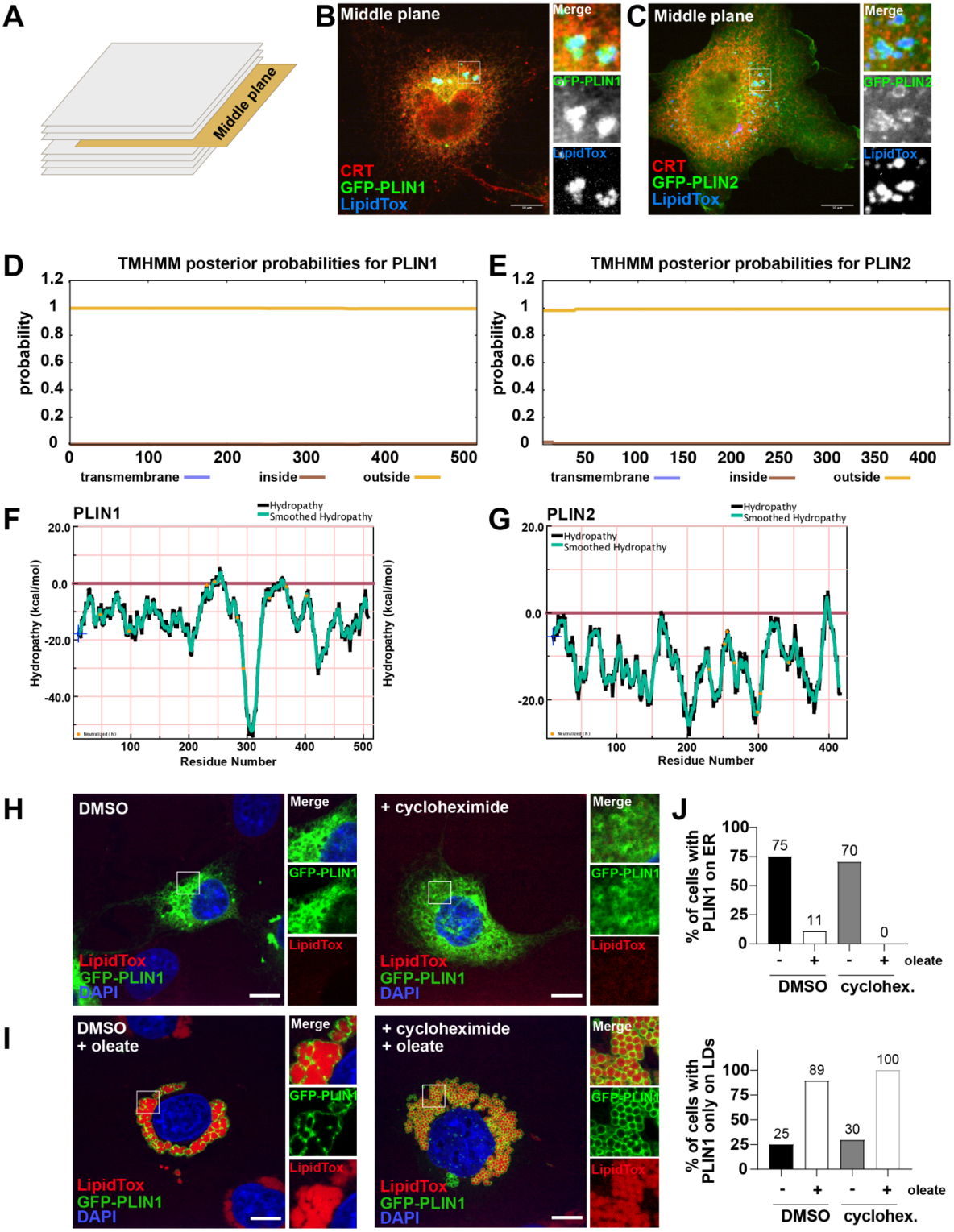


**Figure S2**

693

694 **Figure S2**
695 **Subcellular targeting of PLIN1 and PLIN2;**
696 **TMHMM predictions and hydropathy plot analysis for PLIN1 and PLIN2;**
697 **PLIN1 LD targeting does not require translation.**
698 **(A)** Schematic illustration of image stack and the middle plane shown in (B) and (C).
699 **(B)** COS7 cells expressing PLIN1 tagged at its N-terminus with GFP. Lipid droplets were stained
700 with LipidToxRed and the ER was visualized with an antibody specific to the endogenously
701 expressed luminal ER protein calreticulin (CRT).
702 **(C)** As in (B) but cells expressed PLIN2 with an N-terminal GFP tag (GFP-PLIN2).
703 **(D)** Topology analysis of PLIN1 using TMHMM 2.0 (Trans Membrane prediction Hidden Markov
704 Model[58] https://services.healthtech.dtu.dk/service.php?TMHMM-2.0).
705 No integral membrane domains are predicted. **Outside,** segment in cytoplasm; **Inside,** segment
706 inside the ER lumen; **transmembrane,** integral membrane segment .
707 **(E)** As in (D) but for PLIN2.
708 **(F)** Hydropathy plot analysis for PLIN1 with membrane protein explorer (MPEX)[59].
709 **(G)** As in (F) but for PLIN2.
710 **(H)** COS7 cells expressing PLIN1 tagged at its N-terminus with GFP (GFP-PLIN1). Lipid droplets
711 were stained with LipidToxRed (LipidTox) and nuclei were visualized with DAPI. Cells were
712 either treated with DMSO as a control or with 100µg/ml cycloheximide 7h prior to fixation.
713 Scale bar, 10 µm.
714 **(I)** As in **(H)** but the cells were additionally treated with 200 µM $Na^+$oleate for 6h prior to
715 fixation (1h after addition of DMSO or 100µg/ml cycloheximide). The results are expressed as %
716 of cells with GFP-PLIN1 on LDs.
717 **(J)** Quantification of (H) and (I). The results are expressed as % of cells with GFP-PLIN1 on ER;
718 DMSO: N=20 (-OA), N=28 (+OA); cycloheximide: N=27 (+OA), N=20 (-OA).
719
720
721
722

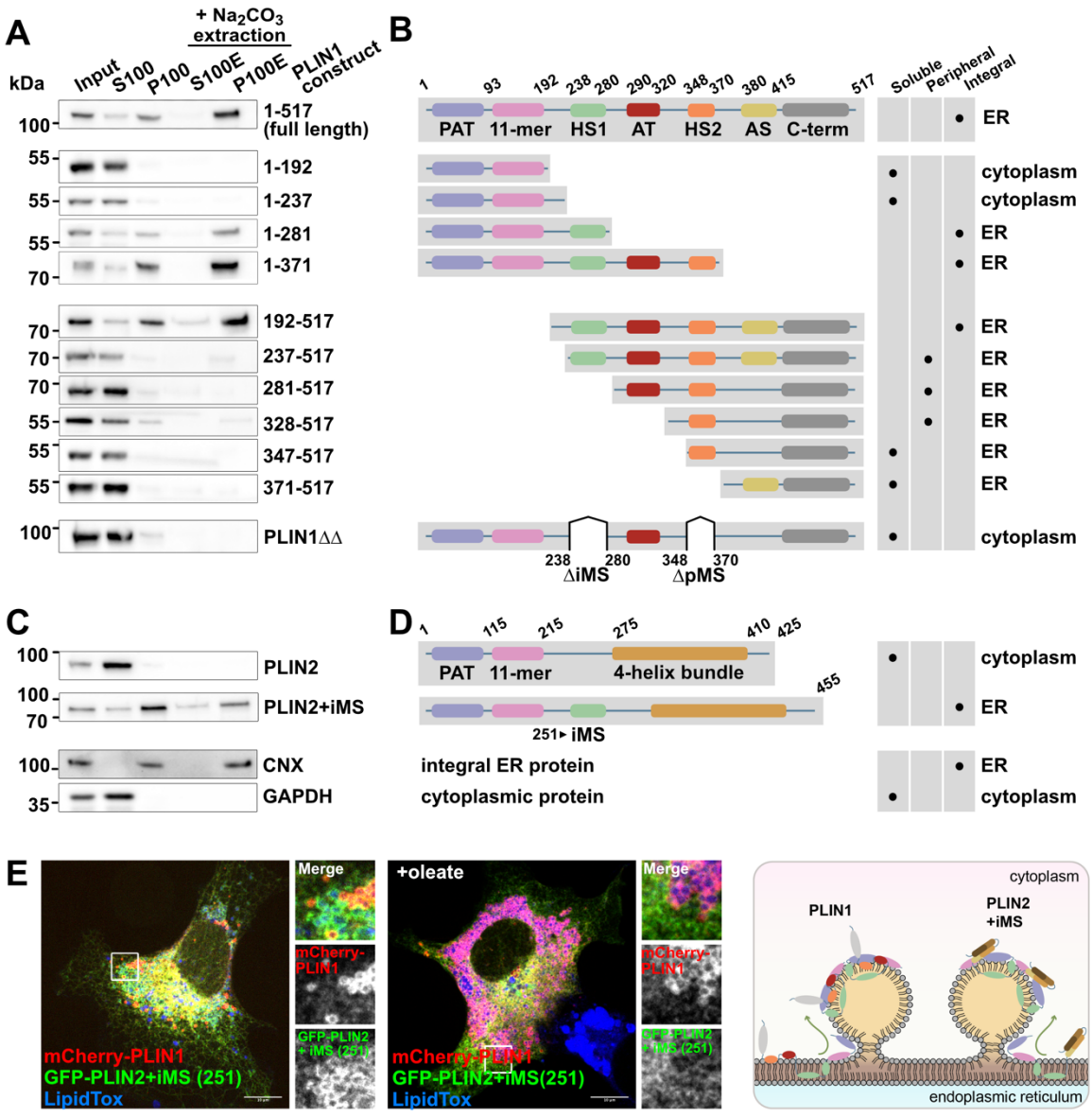


**Figure S3**

723

724 **Figure S3**
725 **Summary of all constructs used in the structure function analysis of PLIN1.**
726 **(A)** Structure-function analysis of PLIN1 by fractionation and alkaline extraction using the
727 indicated truncation constructs.
728 **Input,** cell lysate; **S100, P100,** supernatant and pellet of a 100k x g centrifugation step, **S100E,**
729 **P100E,** supernatant and pellet of 100k x g centrifugation after alkaline extraction with $Na_2CO_3$.
730 Note that PLIN1 1-517 (full length) is also shown in Fig. 2F (GFP-PLIN1) and the constructs 1-
731 237, 1-281 as well as 281-517, 328-517, and 371-517 are shown in main Fig. 3A. PLIN1ΔΔ is also
732 shown in Fig. 3H.
733 **(B)** Schematic illustration of the domains in PLIN1 and the tested truncation constructs. The
734 table summarizes the results in (A) classifying the construct as soluble when found in S100 and
735 in the cytoplasm by microscopy, as peripheral when found in S100, but seen on the ER by
736 microscopy, and integral when present in the alkaline resistant membrane pellet P100E. ER,
737 and cytoplasm is the localization as determined by microscopy. **PAT,** perilipin, adipohilin/ADRP,
738 TIP-47 domain (purple); **11-mer,** LD targeting region (pink); **HS1, 2** hydrophobic segment 1 and
739 2 (green, orange, resp.); **AT,** acidic tract (red); **AS,** amphipathic segment (yellow); **C-term,**
740 carboxy terminus with regulatory elements (grey). Classification of the constructs as soluble,
741 cytoplasmic, peripheral or integral ER membrane proteins.
742 **(C)** Fractionation and alkaline extraction experiments with GFP-PLIN2 (also shown in Fig 2F, for
743 simplicity marked as PLIN2) and GFP-PLIN2 containing the iMS core from PLIN1 inserted after
744 amino acid at position 251. For comparison with fractions in Fig. 2F the cytoplasmic marker
745 **GAPDH,** glycerolaldehyde-3-P-dehydrogenase (from Fig. 2F) and the ER membrane protein
746 marker **CNX,** calnexin (from Fig. 2F) are shown.
747 **(D)** As in (B) but PLIN2 is shown. Classification and definitions as in (B).
748 **(E)** COS7 cells were transfected with PLIN1 tagged at its N-terminus with mCherry2 (mCherry-
749 PLIN1) and PLIN2 containing the iMS core from PLIN1 inserted after amino acid at position 251
750 (GFP-PLIN1+iMS (251). The cells were additionally treated with 250 µM $Na^+$oleate 6h prior to
751 fixation when indicated. The illustration shows that PLIN1 and PLIN2+iMs segregate
752 preferentially to distinct LD classes showing that the iMS is critical in class specific LD nucleation
753 at the ER. Domain colours are as indicated in (B) and (D).
754

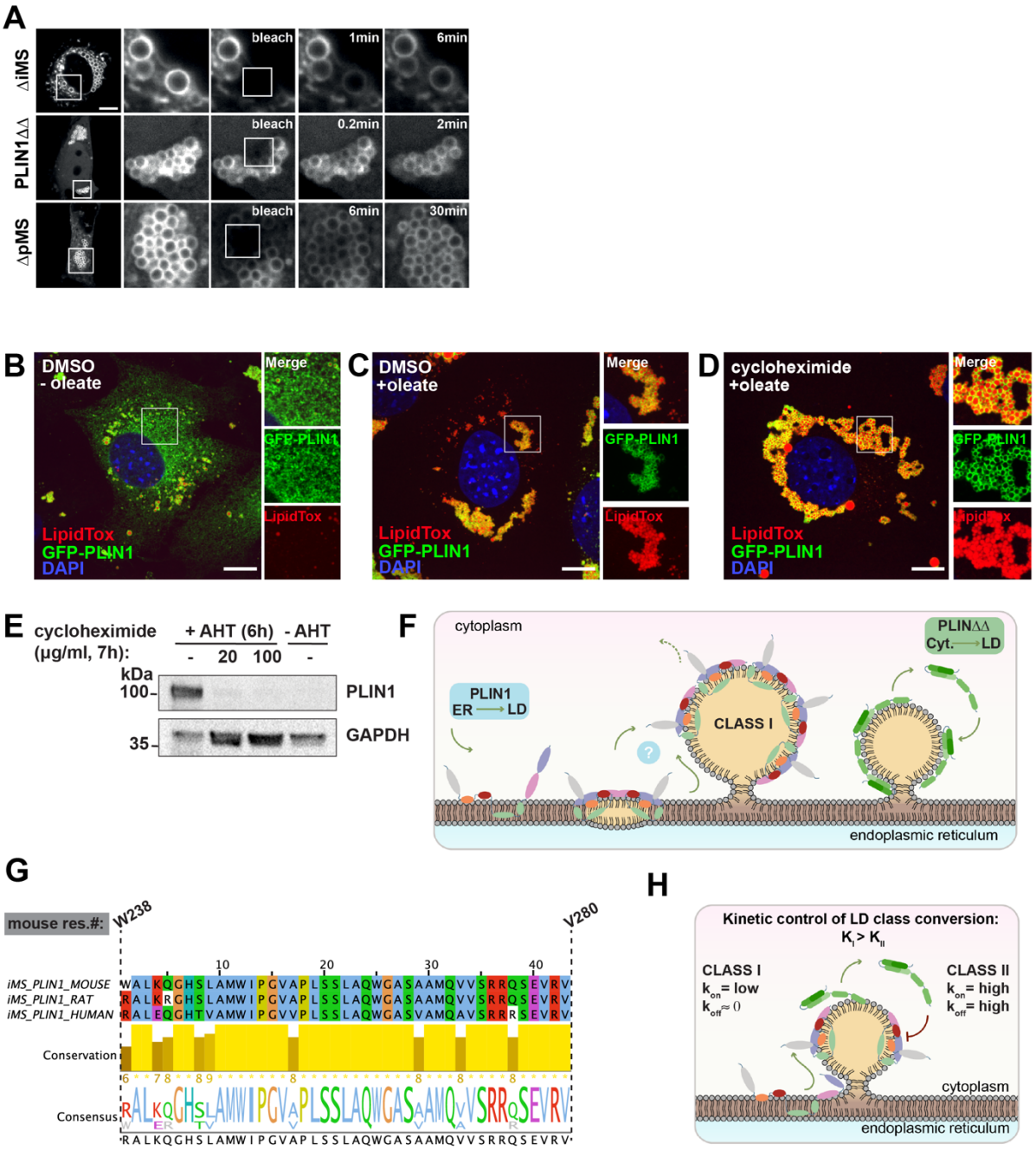


**Figure S4**

755

756
757 **Figure S4.**
758 **Recruitment of PLIN1 from the ER to the LD surface is independent of translation**
759 **(A)** Huh7 cells expressing the indicated GFP-tagged PLIN1 constructs were subjected to
760 photobleaching and the recovery of the GFP signal within the boxed area was plotted over
761 time. **Related to Fig. 4C.**
762 **(B)** 3T3-L1 cells expressing PLIN1 tagged at its N-terminus with GFP (GFP-PLIN1) from a stably
763 integrated inducible trans-gene. Expression was induced with 500 ng/ml anhydrotetracycline
764 (AHT) over-night (total 20h). Lipid droplets were stained with LipidToxRed (LipidTox) and nuclei
765 were visualized with DAPI. Scale bar, 10 µm.
766 **(C)** As in (B) but the cells were additionally treated with $Na^+$oleate 3h prior to fixation.
767 **(D)** As in (C) but translation was shut off by treating the cells with 100 µg/ml cycloheximide 1h
768 before the addition of $Na^+$oleate.
769 **(E)** Validation of GFP-PLIN1 expression and translation shut off by cycloheximide. To induce
770 expression of GFP-PLIN1, the cells were treated with 500ng/ml anhydrotetracycline (AHT) 6h
771 prior to cell harvest. Translation was inhibited with the indicated concentrations of
772 cycloheximide 1h before treatment with AHT. As a negative control AHT was omitted (-AHT).
773 **(F)** PLIN1 is targeted to the ER membrane (brown) by the iMS (green) and the pMS (orange).
774 PLIN1 likely moves to the LD using bridge-connections or by an unknown cytoplasmic
775 intermediate that carries lipids to the LD (indicated by "?"). PLIN1ΔΔ binds to the LD directly
776 from the cytoplasm as expected for a prototypical class-II protein.
777 **(G)** Alignment of mouse, rat and human PLIN1 iMS. The regions correspond to mouse PLIN1
778 residues 238-280. The sequences were retrieved from Uniprot Q8CGN5, P43884, O60240
779 respectively, aligned using ClustalOmega https://www.ebi.ac.uk/Tools/msa/clustalo/ and
780 analysed in JalView https://www.jalview.org/ using the T-coffee algorithm for determination of
781 the consensus sequence shown below the sequence conservation bar graph.
782 **(H)** LD-binding rates of class-II proteins are faster than for class-I proteins. The steady state
783 PLIN1 ER-pool is low, slowing down the LD on-reaction. When bound to the LD, class-II proteins
784 exchange faster than class-I proteins. The resulting high affinity to LDs leads to the gradual
785 replacement of class-II by class-I proteins from the newly formed LDs.
786
787

# Experimental procedures

# STAR Methods

## Lead contact and materials availability

Further information and requests for resources and reagents should be directed to and will be fulfilled by the Lead Contact, Robin Klemm (Robin.Klemm@dpag.ox.ac.uk).

## Data and code availability

Original/source data for in the paper is available upon request from the lead contact and in Supplementary Data.

## Method Details

### Cell lines

COS-7 cells were a kind gift from Tom A. Rapoport (Harvard Medical School, Boston, USA). COS7 is a male African green monkey kidney fibroblast cell line. HEK293T cells were obtained from Dharmacon (#TLP5918). HEK293T is a female human embryonic kidney cell line. 3T3-L1 pre-adipocytes were from ATCC (CL-173). 3T3-L1 is a continuous sub-strain of male murine 3T3 (Swiss albino) cells, developed through clonal isolation.

### Cell culture

COS-7 cells were maintained in Dulbeccos's Modified Eagle Medium with 4.5 g/l glucose and L-glutamine (DMEM, Thermo Fischer Scientific, #41965062), supplemented with 10% fetal bovine serum (FBS; Sigma-Aldrich, #F7524). HEK293T cells were maintained in DMEM containing 10% FBS, 25 mM HEPES (Sigma-Aldrich, H4034), 1 mM sodium pyruvate (Thermo-Fisher), 2 mM glutamine (Sigma-Aldrich) and 100 µM non-essential amino acids (Thermo-Fisher). All cells were kept as sub-confluent cultures and were sub-cultured regularly. All cell lines were periodically tested for mycoplasma and grown according to ATCC guidelines. Cells were incubated at 37°C and 5% $CO_2$.

### Pre-adipocyte maintenance

3T3-L1 pre-adipocytes were obtained from ATCC (CL-173) and cultured in DMEM with 4.5 g/l glucose and L-glutamine (Thermo Fischer Scientific, #41965062), containing 10% calf serum (CS; Sigma-Aldrich, #12133C). Cells were grown as sub-confluent cultures in 10 cm tissue culture dishes (TPP) and sub-cultured regularly.

### Adipocyte differentiation procedure

For the differentiation of 3T3-L1 pre-adipocytes into white adipocytes, the cells were first grown to confluence and kept as a confluent culture for 48 hours. For differentiation in 96-well format, cells were seeded at a density of 10,000 cells per well of a 96-well plate (Greiner). Typically, the cells reached confluence the next day. After 48 hours of confluence differentiation was induced by the addition of adipocyte differentiation medium consisting of DMEM supplemented with 10% FBS, 172 nM bovine insulin (Sigma-Aldrich, #I0516), 500 µM 3-

827 Isobutyl-1-methylxanthine (IBMX, Sigma-Aldrich #I5879), and 1 µM dexamethasone
828 (Gbiosciences, #API-04). Cells were kept in differentiation medium for 48 hours. The
829 differentiation medium was then replaced by DMEM containing 10% FBS and 172 nM bovine
830 insulin. Cells were kept in the insulin medium for another 48 hours. At day four after induction
831 of differentiation the insulin medium was replaced by DMEM containing 10% FBS. The medium
832 was then refreshed every two days. Typically, cells were used for experiments at day 6 or day 8
833 after start of differentiation.
834

835 ## Method details

836 ### Transfection and subcellular fractionation and alkaline extraction

837 $1.1\times10^6$ COS-7 cells were seeded on a 10 cm dish the one day before transfection. The next
838 morning cells were transfected with 10 µg of the plasmid of interest using GeneJuice
839 transfection reagent (Merck, #70967-3) according to the manufacturer's instructions. After 6
840 hours of incubation at 37°C the medium was replaced with fresh DMEM containing 10% FBS.
841 The cells were then incubated at 37°C/5% $CO_2$ overnight. The next morning the cells were
842 washed once with ice-cold PBS and then harvested in 1 mL PBS with a cell scraper. The cells
843 were briefly pelleted at 2000 g for 5 min at 4˚C, and the supernatant was discarded. The cells
844 were resuspended in 1 mL PBS containing protease inhibitor cocktail (cOmplete™, Mini, EDTA-
845 free Protease Inhibitor Cocktail; Merck, #11836153001) (PBSI) and lysed by 20 passages
846 through a bead-homogenizer (Isobiotec, 16 µm bead). A small aliquot for subsequent analysis
847 by SDS-PAGE was taken ("Input") and the remaining lysate was clarified by centrifuging for 10
848 minutes at 4°C and 2000 g. The supernatant was transferred to a 1.5 mL ultracentrifuge tube
849 (Beckman-Coulter, #357448) and the membranes were pelleted at 100,000 g for one hour at
850 4°C in a TLA 100.3 rotor (Beckman-Coulter). Afterwards the supernatant was taken off and
851 stored at -20°C ("S100") and the pellet was resuspended in 50 µL PBSI. A small aliquot of 25 µL
852 was stored at -20°C for analysis by SDS-PAGE ("P100") and the remaining 25 µL were subjected
853 to alkaline extraction by adding 75 µL of 250 mM $Na_2CO_3$ (pH 11) (Sigma Aldrich,
854 #A0634292404) for 15 min on ice. The sample was transferred to a 250 µL ultracentrifuge tube
855 (5 x 20 mm Beckman-Coulter, #342630) and a 50 µL of 10% sucrose cushion was placed below
856 the sample at the bottom of the tube. The samples were then centrifuged for 1 h at 100,000 g
857 and 4°C in a TLS 55 rotor (Beckman-Coulter) with the appropriate adapters (#358614). The top
858 200 µL were carefully taken off and stored at -20°C ("S100E") and the pellet was resuspended in
859 50 µL PBS and stored at -20°C ("P100E"). The samples were subsequently analyzed by SDS-PAGE
860 and western blotting to PVDF membranes (see respective sections).

861 ### Denaturing SDS polyacrylamide gel electrophoresis (PAGE) and immunoblotting

862 SDS-PAGE analysis was carried out either with 10% gels (TGX FastCast acrylamide Kit 10%; Bio-
863 Rad) or precast 4-15% gradient gels (Mini-PROTEAN TGX precast gel; Bio-Rad). The protein
864 concentration was determined using the Pierce 660 nm protein assay (Thermo-Fisher). Samples
865 were denatured by the addition of SDS sample buffer (62.5 mM Tris-HCl, pH 6.8, 10% glycerol,
866 2% SDS, 0.002% bromophenol blue, 5% β-mercaptoethanol) and boiled for 10 minutes at 95°C.
867 For western blotting the proteins were transferred to polyvinylidene difluoride (PVDF)

868 membranes using the Trans-Blot Turbo RTA Mini PVDF Transfer Kit (Bio-Rad) and the Trans-Blot
869 Turbo Transfer System (Bio-Rad). Membranes were blocked for one hour in 3% BSA/TBST (20
870 mM Tris-HCl, pH 7.4, 137 mM NaCl, 0.1% Tween 20) at room temperature. The incubation with
871 the primary antibody was carried out in 3% BSA/TBST either for 1h at room temperature or
872 overnight at 4°C. After extensive washing with TBST the membranes were incubated with the
873 secondary HRP-conjugated antibodies diluted in 5% skim milk/TBST for 1h at room
874 temperature. The membranes were again extensively washed with TBST and the ECL reagent
875 (GE Healthcare) was mixed and added for 1 min afterwards. Images were acquired using Vilber-
876 Lourmat instrument and its software.
877

878 **Lipid droplet flotation**

879 One 10 cm dish of day 6 3T3-L1 adipocytes was used. The cells were washed with ice-cold PBS
880 and subsequently harvested by scraping in PBS. The cells were centrifuged at 600 g, 4°C for 5
881 minutes. The supernatant was discarded, and the pellet containing the cells was resuspended in
882 1 mL PBS supplemented with protease inhibitor (cOmplete™, Mini, EDTA-free Protease
883 Inhibitor Cocktail; Merck). The cells were lysed by 20 passages through a bead homogenizer (16
884 µm bead, Isobiotec) and the lysate was clarified at 600 g, 4°C for 10 minutes. The supernatant
885 was transferred to a new 1,5 mL tube and supplemented with 60% sucrose/PBS to a final
886 concentration of 12% sucrose. 600 µL of the lysate were transferred to an ultracentrifuge tube
887 (5 x 41 mm, Beckman-Coulter, #344090) and centrifuged in an MLS-50 rotor (Beckman-Coulter)
888 at 100,000 g, 4°C for 1h. After the centrifugation the tubes were sealed, and the lower
889 boundary of the floating lipid droplet fraction was marked. The tubes were flash frozen in liquid
890 nitrogen and the top and were collected by cutting the frozen tube. The middle fraction was
891 collected after thawing and the remaining pelleted fraction was washed once with PBS and
892 then resuspended in PBS. All samples were then stored at -20°C until further analysis by SDS-
893 PAGE.

894 **Membrane flotation**

895 Flotation experiments were carried out using five 10 cm dishes COS7 cells. Cells were washed
896 with ice-cold PBS and subsequently harvested by scraping in PBS. The cells were briefly pelleted
897 at 600 g, 4°C for 5 minutes. The supernatant was discarded, and the pellet was resuspended in
898 1 mL PBS supplemented with protease inhibitor (cOmplete™, Mini, EDTA-free Protease
899 Inhibitor Cocktail; Merck). The cells were lysed by approx. 20 passages through a bead
900 homogenizer (Isobiotec, 16 µm bead) and the lysate was cleared from debris at 600 g, 4°C for
901 10 minutes. 100 µL supernatant was collected and stored at -20°C; the remaining supernatant
902 was transferred to a 1.5 mL ultracentrifuge tube (Beckman-Coulter) and centrifuged in a
903 TLA 100.3 rotor (Beckman-Coulter) at 100,000 g, 4°C for one hour. The supernatant was
904 transferred to a new 1.5 mL tube and stored at -20°C for later analysis. The pellet was
905 resuspended in 36 µL PBS supplemented with protease inhibitor and 10 µL were stored for later
906 analysis at -20°C. The remaining 26 µL were supplemented with 150 µL of 60% sucrose (w/v). To
907 remove the ribosomes from the membranes 24 µL puromycin (10 mg/mL) were added to a final
908 concentration of 2,5 M puromycin and 45% sucrose. The reaction was incubated at RT for 30
909 minutes. 300 µL of 35% sucrose (w/v) were added to a 600 µL ultracentrifuge tube (Beckman-
910 Coulter) and the resuspended pellet fraction in 45% sucrose (w/v) was loaded to the bottom of

911 the tube. Finally, 150 µL of 5% sucrose (w/v) were pipetted on top, the interphases were
912 marked, and the sample centrifuged in a MLS 50 rotor (Beckman-Coulter) at 150,000 g, 4°C for
913 3h. The tubes were subsequently frozen in liquid nitrogen and the fractions separated by
914 cutting the tube at the interface marks using a clean scalpel. The fractions that were collected
915 are the top fraction with 5% sucrose, the interphase between 5% and 35% sucrose, the 35%
916 sucrose fraction, the interphase between 35% and 45% sucrose and the bottom fraction with
917 45% sucrose. The protein concentration of the fractions was determined, and equal amounts
918 analyzed by SDS-PAGE.

919 **Indirect immunofluorescence**

920 For indirect immunofluorescence experiments cells were trypsinized and transferred either to
921 Ø 18 mm cover glasses (No. 1; VWR) in 12-well tissue culture plates (TPP) or to 96-well plates
922 (Greiner) and cultured using DMEM supplemented with 10% of the respective serum (calf
923 serum CS for 3T3-L1 or FBS for COS7 and differentiated adipocytes). Differentiated adipocytes
924 were cultured for at least two days after trypsinization to ensure proper settling of the cells.
925 Cells were fixed with 4% paraformaldehyde (PFA; Electron Microscopy Sciences) at 37°C for 30
926 minutes. After washing three times with PBS, cells were permeabilized for 15 minutes either
927 with 0.1% Triton-X100 in PBS, or, when PLIN2 or PLIN3 or 4 were stained in adipocytes, 0.2%
928 saponin and 1% CS in PBS. Cells were again washed and incubated with primary antibodies in
929 blocking solution (PBS supplemented with 1% CS) for 1 h at RT. After washing, the cells were
930 incubated with fluorescently labeled secondary antibodies in blocking solution for 1h at RT. For
931 lipid droplet visualization HCS LipidTOX™ Green/Red/Deep Red dyes (Thermo-Fisher,
932 #H34475/#H34476/3H34477, respectively) were used at 1:500 dilution in PBS. Nuclei were
933 counterstained using DAPI (Thermo-Fisher) at a concentration of 0.4 µL/mL for 10 minutes at
934 RT. Cell outline staining, if applied, was done using Atto 490LS NHS-Ester (ATTO-TEC) at a
935 dilution of 1:800,000 in carbonate buffer for five minutes at RT.
936 Cover glasses were mounted onto Superfrost Excell glass slides (Thermo-Fisher) using
937 Fluoromount G (SouthernBiotech). Image acquisition was performed as described under
938 "Microscopy".

939 **Determination of protein concentration**

940 Protein concentration was determined in 96-well plates using the Pierce™ 660nm Protein Assay
941 (Thermo-Fisher) according to the manufacturer's manual. A standard-curve was produced with
942 a BSA solution ranging from 50-2000 µg/mL.
943

944 **Microscopy**

945 Confocal fluorescent microscopy was done on a Nikon Eclipse Ti-E microscope with enhanced
946 CSU-W1 spinning disk (Microlens-enhanced dual Nipkow disk confocal scanner, wide view
947 type), a Nikon CFI PlanApo 100x oil immersion objective (NA 1.49), and a sCMOS PCO Edge 5.5
948 camera (PCO, 2560x2160 pixels).
949 For automated confocal microscopy a Yokogawa CellVoyager 7000 spinning disk confocal
950 microscope with enhanced CSU-X1 spinning disk (Microlens-enhanced dual Nipkow disk
951 confocal scanner, wide view type), a 40x air objective (NA 1,15) or 60x water immersion (NA
952 1,2), and three Neo sCMOS cameras (Andor, 2560x2160 pixels) were used. 108 sites were

953 acquired per well of a 96-well plate with seven confocal planes of 1 µm thickness per site,
954 which were maximum intensity projected before saving. The signals for UV (405 nm) and far-
955 red (640 nm) as well as green (488 nm) and Atto490LS (675 nm) signals were acquired in dual-
956 camera mode. Red signal (561 nm) was acquired separately.
957 Images for parts of Fig. 4, S4 and S2H-I were captured on an Olympus SpinSR10 spinning disc
958 confocal system fitted with an Olympus IX-83 frame, a Yokogawa CSU-W1 SoRa super-
959 resolution spinning disc module, a Photometrics Prime BSI camera and a 60× objective (1.5 NA,
960 UPLAPOHR60x), using Olympus cellSens Dimension software. When indicated the images were
961 post-processed using an OSR filter (standard) and deconvolved (constrained iterative, maximum
962 likelihood, 5 iterations) using Olympus cellSens Dimension software (version 3.1.1).
963

964 **Automated image analysis**

965 The acquired images were analyzed using CellProfiler (https://cellprofiler.org/). When
966 necessary the cell profiler pipelines were run on the high-performance cloud computing system
967 "ScienceCloud" at the University of Zurich. Analysis pipelines were composed of generic or
968 partially customized modules as described in (Battich, Stoeger, & Pelkmans, 2015). Individual
969 cells were segmented with nuclei as primary objects that were identified based on DAPI signal,
970 and cell outlines were determined from Atto490LS signal using iterative segmentation based on
971 a watershed algorithm and related to nuclei as secondary objects. After cell segmentation the
972 background of all stainings of interest was subtracted and single-cell based features like area,
973 shape, intensities and textures were extracted using the modules "MeasureObjectAreaShape",
974 "MeasureObjectIntensity", and "MeasureTexture". Subsequent analysis was done with Matlab
975 (Mathworks).

976 **Single cell classification by support vector machines (SVMs)**

977 Single cells were classified using user supervised machine learning with a custom Matlab script
978 CellClassifier (Rämö, Sacher, Snijder, Begemann, & Pelkmans, 2009). The classifier is based on
979 support vector machine algorithm (SVM). In general, the classifiers were trained to identify and
980 remove cells that were miss-segmented using nuclear area, nuclear shape, intensity, and
981 textures as training features. Cells which overlapped with the border of an individual imaging
982 site were automatically identified and removed. Furthermore, experiment specific SVMs were
983 trained using intensity, channel correlation and texture as training features.
984

985 **Cloning of truncations and deletion mutants**

986 All truncation- and deletion-mutants were cloned by restriction ligation into the mEGFP-C1
987 using *Hind*III and *Kpn*I restriction sites. The mEGFP-C1 plasmid was a kind gift from Michael
988 Davidson (Addgene plasmid #54759).
989

990 **Cloning of GFP-PLIN2-251InsIMs**

991 Cloning of the PLIN2 domain swap mutant carrying the core iMS (PLIN1 amino acids 238-268) of
992 PLIN1 was done by insertion of the iMS sequence into mEGFP-C1-PLIN2 after amino acid 251 of
993 the PLIN2 sequence. The insertion was done using the Q5 Site-Directed Mutagenesis Kit (NEB)

994 and design of respective primers using the NEBaseChanger online tool (http://
995 nebasechanger.neb.com/).
996
997 **Generation of stable cell line inducibly expressing GFP-PLIN1**

998 The stable 3T3-L1 cells with inducibe GFP-PLIN1 or GFP-PLIN1ΔΔ (Δ238-280-Δ348-370),
999 respective transgenes were generated by lentiviral gene transfer using the pINDUCER20
1000 construct and Gateway™ cloning technology. The pInducer20 was a kind gift from Stephen
1001 Elledge (Addgene #44012). The respective transgenes were first sub-cloned by TOPO cloning
1002 into a Gateway™ entry vector (pENTR™/D-TOPO™; Thermo-Fisher) and subsequently
1003 recombined into the pINDUCER20 vector using the Gateway™ LR Clonase™ II Enzyme mix
1004 (Thermo-Fisher). Production of lentiviruses and transduction of cells was performed as
1005 described below.
1006 The cell lines were subsequently established by selecting positively transduced cells using G418
1007 selection (1 mg/mL) for several passages.
1008 Expression of the respective transgene was usually induced with 500 ng/mL
1009 anhydrotetracycline (ATC) for the indicated time-frames.
1010
1011 **Preparation of sodium oleate**

1012 To prepare a solution of sodium oleate, 30 mL of double-distilled water were warmed up in the
1013 microwave to approx. 40°C and 400 µL of 5 M NaOH were added. While constantly stirring, 400
1014 µL of oleic acid (Sigma-Aldrich) were slowly added and the solution was stirred for another five
1015 minutes (stock concentration 41 mM). If micelles where still visible, additional NaOH was added
1016 until all micelles disappeared. The solution was sterile filtered through a 0.22 µm sterile filter,
1017 aliquoted and stored at -20°C. Using 147 µL of the solution per 25 mL of culture medium
1018 resulted in a final concentration of 250 µM.
1019
1020 **Cell treatments**

1021 Lipolysis was induced in differentiating adipocytes by addition of 1 mM forskolin in the medium
1022 (or vehicle, DMSO) to the final concentration of 10µM, for 6 hours. Oleate uptake was done by
1023 adding sodium oleate to the medium in the indicated concentration for 6 hours. Protein
1024 synthesis was inhibited by incubating cells in the medium containing cycloheximide (or DMSO
1025 control) to final concentration of 100µg/ml for the indicated time.
1026
1027 **Cover glasses acid wash**

1028 Cover glasses (Ø 18 mm; VWR No. 1) were placed in a ceramic rack and submerged in 2 M HCl
1029 for 15 minutes. The coverslips were rinsed under tap water for 30 minutes and then washed
1030 three times with double-distilled water. Finally, the coverslips were rinsed in ethanol, sterilized
1031 under UV-light for 30 minutes and stored in a closed container in a tissue culture hood.
1032
1033 **Production of lentivirus for gene transfer**

1034 Lentivirus for gene transfer and integration of pINDUCER constructs was produced in HEK 293T
1035 cells (Dharmacon). The cells were cultured in DMEM supplemented with 10% FBS, 25 mM

1036 HEPES (Sigma-Aldrich, H4034), 1 mM sodium pyruvate (Thermo-Fisher), 2 mM glutamine
1037 (Sigma-Aldrich) and 100 µM non-essential amino acids (Thermo-Fisher) on 10 cm dishes until
1038 reaching approx. 70% confluency. The cells were transfected using the calcium phosphate
1039 method with the three components necessary for the lentiviral packaging: 10 µg of the
1040 pINDUCER expression vector containing the construct of interest, 6.5 µg psPAX2 (Addgene #
1041 12260), the viral genome packaging plasmid, and 3.5 µg pMD2.G (Addgene # 12259), encoding
1042 for the viral envelope components were gently mixed with $H_2O$ to a total volume of 597 µl. This
1043 was mixed with 682 µl 2x HBSS (Hank's Balanced Salt Solution), and 85 µl 2M $CaCl_2$ were added
1044 followed by 30 min incubation at RT. The entire transfection mix was added dropwise to the
1045 cells and incubated for approx. 12h at 37˚C, 5% $CO_2$. After that the medium was replaced by
1046 DMEM supplemented with 5% FBS. The media containing the lentiviral particles was collected
1047 at 24, 48, and 60 hours after changing the medium. The individual fractions were sterile filtered
1048 through a 0.45 µm filter, pooled and stored at 4°C. The virus particles were then concentrated
1049 to approx. 200 µL final volume using an Amicon Ultra-15 centrifugal filter unit (Merck) with a
1050 molecular weight cut-off of 100 kDa (Amicon "Ultra – 15 centrifugal filter"; 100 kDa MW-cut
1051 off). The filtrate was brought to 1 mL final volume with DMEM supplemented with 10% CS and
1052 immediately used for transduction of 3T3-L1 cells as described below.
1053
1054 **Transduction of 3T3-L1 preadipocytes with lentivirus**

1055 3T3-L1 cells were grown in 6-well plates until 50-60% confluency before the medium was
1056 replaced by the concentrated virus mixture supplemented with 8 µg/mL polybrene (Sigma-
1057 Aldrich, #107689). After overnight incubation the medium was replaced by DMEM
1058 supplemented with 10% CS. Cells were further selected or subjected to single clone dilution as
1059 described below.
1060
1061 **Single cell classification by support vector machines (SVMs)**

1062 Single-cell data obtained after automated image analysis was further analyzed using
1063 CellClassifier (Rämö, Sacher, Snijder, Begemann, & Pelkmans, 2009), a classifier software based
1064 on SVMs for supervised machine learning. In general, for all datasets SVMs were trained to
1065 identify and remove cells that were miss-segmented based on features like nuclear area,
1066 nuclear shape, intensity, and texture features. Also, datasets were automatically cleansed of
1067 cells which touch the border of an individual imaging site. Furthermore, experiment specific
1068 SVMs were trained e. g. for identifying transfected cells or cells which show a specific
1069 phenotype.
1070
1071 **In vitro experiments**

1072 The purification protocol for LDs from cells expressing fluorescently tagged LD proteins was the
1073 same as in Ajjaji et al. 2019. Briefly, cells from 5 x 15 cm dishes were harvested, washed once in
1074 ice-cold PBS, and lysed using a 30G needle in 1ml 20 mM Tris-EDTA buffer containing complete
1075 protease and phosphatase inhibitor tablets at pH 7.5. To isolate LDs, 1ml of respective cell
1076 lysates were mixed with 1 ml 60% sucrose in 20 mM Tris-EDTA buffer supplemented with
1077 protease inhibitors, overlaid with 20%, 10% and 0% in buffered sucrose on top of one another
1078 in 5 ml Ultra-Clear centrifuge tubes (Beckman). Gradients were centrifuged for 16 h at 100,000

1079 x *g* and 4 °C, using an SW60 rotor in a Beckman L8-70 centrifuge, and 300 µL were collected
1080 from the top as the LD fraction.
1081
1082 In vitro experiments were performed in HKM buffer: 50 mM Hepes, 120 mM $K^+OAc$, and 1 mM
1083 $MgCl_2$ (in Milli-Q water) at pH 7.4. To create buffer-in-oil drops, a buffer-diluted LD fraction was
1084 mixed with an excess of triolein by vortexing, as previously done in Ajjaji et al. 2019. The
1085 shrinkage of the buffer compartment was based on water evaporation of the aqueous drops,
1086 with the proteins at their surface, during imaging for 10 to 15 min on PDMS-coated glass slides.
1087
1088

### 1089 Fluorescence recovery after photo-bleaching FRAP experiments

1090 For FRAP experiments, we bleach the signal on a collection of drops and monitor the signal
1091 recovery. The background signal, e.g. from the cytosol, is removed from the recorded signal,
1092 which was at the end normalized by intrinsic bleaching of non-bleached areas. We used
1093 GraphPad Prism to fit the FRAP recovery curves with a non-linear regression and the
1094 exponential « one-phase association model ». The characteristic recovery time is extracted
1095 from the model.
1096

### 1097 Transfections

1098 When indicated Huh7 cells (60-70% confluence) were exposed for 1hr to 500 µM oleic acid
1099 coupled to BSA (1% v:v) to induce LD formation and then cells were transfected with 3 µg of
1100 plasmid DNA/mL using Polyethylenimine HCl MAX (Polysciences, Inc) following the
1101 manufacturer's instructions.
1102

## 1103 Quantification and statistical analysis

1104 Number of samples and replicates in an experiment, as well as dispersion (standard deviation,
1105 SD, standard error of the mean, SEM), are reported for each figure in the respective legends.
1106 Quantification of experimental data are described in relevant Method sections.
1107
1108

1109 ## KEY RESOURCES TABLE

| REAGENT or RESOURCE | SOURCE | IDENTIFIER |
|---|---|---|
| **Antibodies** | | |
| Mouse monoclonal c-Myc, 1:200 | Santa Cruz | Cat#: sc-40 |
| Rabbit polyclonal Calreticulin, 1:1000 | Abcam | Cat#: ab2907 |
| Mouse monoclonal FLAG, 1:200 | Sigma-Aldrich | Cat#: F3165 |
| Mouse monoclonal HA, 1:200 | Roche | Cat#: 11583816001 |
| Goat polyclonal PLIN1, 1:200 | Abcam | Cat#: ab61682 |
| Rabbit monoclonal PLIN1, 1:200 (Fig4 I-M) | Cell Signaling | Cat#: #9349 |
| Rabbit polyclonal PLIN2, 1:200 | Abcam | Cat#: ab52355 |
| Rabbit polyclonal PLIN3, 1:200 | Millipore | Cat#: ABS482 |
| Rabbit polyclonal PLIN4, 1:200 | Sigma-Aldrich | Cat#: ABS526 |
| Rabbit polyclonal Calnexin (CNX), 1:200 | Proteintech | Cat#: 10427-2-AP |
| Rabbit polyclonal CKAP4 (CLIMP63), 1:200 | Bethyl Laboratories | Cat#: A302-257A |
| Donkey anti-goat IgG Alexa Fluor 488, 1:500 | Thermo-Fisher | Cat#: A11055 |
| Donkey anti-goat IgG Alexa Fluor 568, 1:500 | Thermo-Fisher | Cat#: A11057 |
| Donkey anti-goat IgG Alexa Fluor 647, 1:500 | Thermo-Fisher | Cat#: A21447 |
| Donkey anti-mouse IgG Alexa Fluor 488, 1:500 | Thermo-Fisher | Cat#: A21202 |
| Donkey anti-mouse IgG Alexa Fluor 568, 1:500 | Thermo-Fisher | Cat#: A10042 |
| Donkey anti-mouse IgG Alexa Fluor 647, 1:500 | Thermo-Fisher | Cat#: A31571 |
| Donkey anti-rabbit IgG Alexa Fluor 488, 1:500 | Thermo-Fisher | Cat#: A21206 |
| Donkey anti-rabbit IgG Alexa Fluor 568, 1:500 | Thermo-Fisher | Cat#: A10042 |
| Donkey anti-rabbit IgG Alexa Fluor 647, 1:500 | Thermo-Fisher | Cat#: A31573 |
| Donkey anti-goat HRP, 1:2500 | Bethyl | Cat#: A50-201P |
| Donkey anti-mouse HRP, 1:5000 | Promega | Cat#: W4021 |
| Donkey anti-rabbit HRP, 1:5000 | Promega | Cat#: W4011 |
| | | |
| **Biological samples** | | |
| N/A | | |
| **Chemicals, peptides, and recombinant proteins** | | |
| DMEM | GIBCO | Cat#41965-039; CAS/RRID: N/A |
| Fetal bovine serum | Sigma-Aldrich | Cat#F7524; CAS/RRID: N/A |
| Calf serum | Sigma-Aldrich | Cat#12133C; CAS/RRID: N/A |
| OptiMEM | GIBCO | Cat#11058-021; CAS/RRID: N/A |
| Non-essential amino acids | Sigma | Cat#M7145; CAS/RRID: N/A |
| Sodium Pyruvate | GIBCO | Cat#11360 070; CAS: 113-24-6 |
| Puromycin | Invivogen | Cat#ant-pr-1; CAS: 58-58-2 |
| Geneticin G418 | Invivogen | Cat#ant-gn-1; CAS: 108321-42-2 |
| Paraformaldehyde | Electron Microscopy Sciences | Cat#15711; CAS: 50-00-0 |
| Triton X-100 | Thermo Fisher Scientific | Cat#28314; CAS: 9002-93-1 |

| | | |
|---|---|---|
| Hexadimethrine bromide | Sigma-Aldrich | Cat#107689; CAS: 28728-55-4 |
| Oleic Acid | Sigma-Aldrich | Cat#O1383-5G; CAS: 112-80-1 |
| HCS LipidTOX Red Neutral Lipid Stain | Thermo-Fisher | Cat#H34476; CAS: N/A |
| HCS LipidTOX Deep Red Neutral Lipid Stain | Thermo Fisher Scientific | Cat#H34477; CAS: N/A |
| Fluoromount-G | SouthernBiotech | Cat#0100-01; CAS: 0100-01 |
| Dexamethasone | G-Biosciences | Cat#API-04; CAS: 50-02-2 |
| 3-Isobutyl-1-methylxanthine | Sigma-Aldrich | Cat#I5879; CAS: 28822-58-4 |
| Insulin | Sigma-Aldrich | Cat#I0516-5ML; CAS: 11070-73-8 |
| Cycloheximide | Sigma-Aldrich | Cat#C7698; CAS: 66-81-9 |
| Forskolin | Sigma-Aldrich | Cat#F3917-10MG; CAS: 66575-29-9 |
| Atto490LS NHS Ester | Atto-tec | Cat#AD 490LS-31; CAS/RRID: N/A |
| Alexa Fluor 647 NHS Ester | Life Technologies | Cat#SE-af647; CAS/RRID: N/A |
| cOmplete, Mini Protease Inhibitor Cocktail | Sigma Aldrich | Cat#11836153001; CAS/RRID: N/A |
| Ionic Detergent Compatibility Reagent for Pierce | Thermo Fisher Scientific | Cat#22663; CAS/RRID: N/A |
| D-Glucose [U-14C] | Hartmann analytic | Cat#MC 144W; CAS/RRID: N/A |
| Doxycycline hyclate | Sigma-Aldrich | Cat#D9891-1G; CAS: 24390-14-5 |
| Chloroform | Rathburn Chemicals | Cat#RH1009; CAS: 67-66-3 |
| Methanol | Biosolve Chemicals | Cat#13687802; CAS: 67-56-1 |
| Propanol | Sigma-Aldrich | Cat#650447; CAS: 67-63-0 |
| | | |
| **Critical commercial assays** | | |
| Pierce 660nm Protein Assay Reagent | Thermo Fisher Scientific | Cat#22660; CAS/RRID: N/A |
| GFP-Trap Magnetic Agarose | ChromoTek | Cat# gtma-10 |
| | | |
| **Deposited data** | | |
| Mouse 3T3-L1 cells | ATCC | Cat#CL-173; RRID: CVCL_0123 |
| Monkey COS-7 cells | Tom A. Rapoport, Harvard Medical School, Boston, USA | N/A; RRID: CVCL_0224 |
| Human HEK293T cells | Dharmacon | Cat#TLP5918; RRID: CVCL_0063 |
| | | |
| **Experimental models: Cell lines** | | |
| COS-7 | Tom A. Rapoport (Harvard Medical School, Boston, USA) | |

| | | |
|---|---|---|
| 3T3-L1 | ATCC | CL-173 |
| HEK293T | Dharmacon | |
| | | |
| **Experimental models: Organisms/strains** | | |
| N/A | | |
| **Oligonucleotides** | | |
| Cloning primers for GFP-PLIN1 mutations | This study | Supplementary Table |
| | | |
| **Recombinant DNA** | | |
| mEGFP-N1 | Michael Davidson Lab | Addgene 54767 |
| mEGFP-C1 | Michael Davidson Lab | Addgene 54759 |
| mCherry2-C1 | Michael Davidson Lab | Addgene 54563 |
| mCherry2-N1 | Michael Davidson Lab | Addgene 54517 |
| pINDUCER20 | Stephen Elledge Lab | Addgene 44012 |
| pINDUCER21 | Stephen Elledge & Thomas Westbrook Lab | Addgene 46948 |
| APEX2-GBP | Rob Parton Lab | Addgene 67651 |
| psPAX2 | Didier Trono Lab | Addgene 12260 |
| pMD2.G | Didier Trono Lab | Addgene 12259 |
| GFP-PLIN1 | This study | N/A |
| GFP-PLIN2 | This study | N/A |
| GFP-PLIN3 | This study | N/A |
| GFP-PLIN1 1-92, 1-237, 1-281, 1-371 | This study | N/A |
| GFP-PLIN1 192-517, 237-517, 281-517, 328-517, 347-517, 371-517 | This study | N/A |
| GFP-PLIN1-ΔΔ (Δ238-280 Δ348-370) | This study | N/A |
| GFP-PLIN2+251InsiMS | This study | N/A |
| cDNA Mouse PLIN1 | Dharmacon | MMM1013-202799812 |
| cDNA Mouse PLIN3 | Dharmacon | MMM1013-202764453 |
| | | |
| **Software and algorithms** | | |
| MATLAB | | https://www.mathworks.com/products/matlab.html |
| CellProfiler | Carpenter et al., 2006 | https://github.com/pelkmanslab/CellProfilerPelkmans |
| CellProfiler Pelkmans Lab | Battich et al., 2015 | https://github.com/pelkmanslab/CellProfilerPelkmans/tree/master/Modules |
| ImageJ | National Institutes of Health, USA | https://imagej.net/Welcome RRID: SCR_003070 |
| | | |
| **Other** | | |
| Round microscope cover glasses, 18 mm, No. 1 | VWR | Cat#631-1580; CAS/RRID: N/A |
| Nikon Eclipse Ti E with CSU-W1 spinning disk | Nikon | |
| Yokogawa CellVoyager 7000 with CSU-X1 spinning disk | Yokugawa | |
| Leica SP5 confocal laser scanning microscope | Leica | |

1110